



# Investigation on the hot corrosion behavior of a single crystal Ni-based superalloy in molten $\text{Na}_2\text{SO}_4 + \text{K}_2\text{SO}_4$ salts improved by different preoxidation treatments

Xiaowen Yang<sup>a</sup>, Lanlan Yang<sup>b</sup>, Jinlong Wang<sup>a,\*</sup>, Zehao Chen<sup>a</sup>, Minghui Chen<sup>a</sup>, Jianqiang Zhang<sup>c</sup>, Fuhui Wang<sup>a</sup>

<sup>a</sup> Shenyang National Laboratory for Materials Science, Northeastern University, Shenyang 110819, China

<sup>b</sup> School of Materials Science and Engineering, Jiangsu University of Science and Technology, Zhenjiang 212003, China

<sup>c</sup> School of Materials Science and Engineering, UNSW Sydney, Australia

## ARTICLE INFO

### Keywords:

- A. Superalloys
- C. Oxidation
- C. Hot corrosion

## ABSTRACT

This study investigated the hot corrosion behavior of N5 in molten sulfate at 850 °C after different peroxidation treatments. The preoxidation was conducted at 900, 1000 and 1100 °C for 20 and 100 h, respectively. The preformed oxide scale featured a multilayered structure and varying degrees of Ta oxides. Among all, the samples preoxidized at 900 °C exhibited the highest corrosion resistance. But a porous structure with a large number of internal oxides and sulfides was observed when preoxidized at 1000 and 1100 °C. The alloy without preoxidation directly reacted with the molten salt to form a porous structure with internal oxides and sulfides.

## 1. Introduction

Hot corrosion has become a key problem restricting the service capacity of turbine blade materials, which usually results from sulfate deposits generated by the oxidation or combustion of sulfur and alkaline metal-containing impurities in fuel and aerosols in the air [1–4]. The occurrence of hot corrosion tends to accelerate oxidation and cause the failure of superalloys used for turbine blades [5,6]. The elevated temperature used in this application higher than the melting point of the sulfate makes the salt deposits in the form of a molten state. This type of corrosion is classified as Type I hot corrosion (800–950 °C) [7,8]. Type I hot corrosion can be attributed to a fluxing process in which the chemistry modification of the molten salts can dissolve the surface protective oxide scale. As the scale is destroyed, the molten salts access and penetrate into the substrate alloy; thus, the produced oxygen and sulfur penetrated into the matrix and directly react with the beneficial alloy elements such as Al and Cr to form internal oxidation and sulfidation. With the combination process involved in both scale dissolution and internal corrosion proceeding, the surface scale becomes defective and non-protective. Thereafter, accelerated and destructive corrosion failure is triggered [9–11].

Hot corrosion has been extensively studied for single-crystal (SC)

nickel-based superalloys due to their excellent high-temperature in-service properties [7,8,12–14]. Eliminating grain boundaries and introducing more refractory elements increase the high-temperature mechanical properties. However, refractory elements such as W and Mo and their oxides can strongly react with molten salts (mainly consume O<sup>2-</sup> from SO<sub>2</sub> – 4), which leads to an acidic environment near the alloy/salt interface and promotes the protective oxides on the alloy surface decomposing. Consequently, a more aggressive acidic fluxing of corrosion proceeds. Therefore, the resistance to hot corrosion at high temperatures is even more critical for SC Ni-based superalloys.

It has been widely reported that hot corrosion problems can be reduced by the application of protective coatings [15–19], which is attributed to the formation of a dense intact scale of Al<sub>2</sub>O<sub>3</sub> or Cr<sub>2</sub>O<sub>3</sub>. The protective scale can prevent oxygen, sulfur and other ions from penetrating the substrate and thus improve corrosion resistance [12,15]. As the corrosion process proceeds, apparent Al/Cr-depletion and significant interdiffusion will limit the in-service properties of the coating/alloy. Another method of preoxidation technology has been developed to retard corrosion by performing a protective scale on the alloy surface. It has been reported by Chen et al. [20] that preoxidation of CoNiCrAlYRe alloy rendered it to form dense multiple layers of oxide scale (Al<sub>2</sub>O<sub>3</sub> and Cr<sub>2</sub>O<sub>3</sub>) on the surface, thereby effectively preventing

\* Corresponding author.

E-mail address: [Wangjinlong@mail.neu.edu.cn](mailto:Wangjinlong@mail.neu.edu.cn) (J. Wang).

sulfur from penetrating the substrate and benefiting its anticorrosion ability by prolonging the incubation time. Similarly, it has been proven by Liu et al. [21] that the formation of a continuous scale of  $\text{Cr}_2\text{O}_3$  and spinels for the Ni-based superalloy M38G preoxidized at 950 °C could inhibit the subsequent hot corrosion in 75 wt%  $\text{Na}_2\text{SO}_4$  + 25 wt%  $\text{NaCl}$  salts at 800 °C and 850 °C to some extent. Nevertheless, Liu et al. [22] reported that multiple oxides formed for the DZ68 Ni-based superalloy preoxidized at 950 °C for 20 h. However, such a pretreatment could not alleviate hot corrosion at 900 °C in molten sulfate salts but instead increase the corrosion rate. The stability of the preformed scale and its effectiveness on hot corrosion are affected by many factors, e.g. alloy composition, reaction temperature and time, etc. which however, is still not very clear. Therefore, the preoxidation process needs to be systematically investigated for this application.

For most nickel-based superalloys, the oxide products are mainly composed of  $\text{NiO}$ ,  $\text{Ni-Al/Cr}$  spinel and  $\text{Al}_2\text{O}_3$  when oxidized at temperatures above 900 °C [23–26]. This becomes more complicated for SC superalloys. Taking the 2nd SC superalloy René N5 as an example, Ta oxides would form after just short-term oxidation, which influences the integrity of the whole oxide scale. It is worth noting that research on the Ta effect on oxidation and hot corrosion behavior has attracted increasing attention in recent years, especially on SC substrates [27–29]. However, the role of Ta in hot corrosion is still unclear. It has been reported that Ta plays a beneficial role in improving corrosion resistance by promoting the formation of  $\text{NaTaO}_3$  and  $\text{TaS}_2$ , which suppresses the formation of liquid phases of  $\text{Na}_2\text{Mo}(\text{W})\text{O}_4$  and Ni sulfides [30,31]. Chang et al. [32] reported that an optimum Ta/Cr(wt%) ratio promoted the formation of continuous  $\text{Cr}_2\text{O}_3$  and Ta-containing spinel at 900 °C, which retarded the diffusion of ions. Therefore, the corrosion resistance of the alloy is improved by Ta addition based on these reports. In contrast, the results acquired by other researchers demonstrated that Ta deteriorated the hot corrosion resistance by forming  $\text{NaTaO}_3$ , which led to pits and provided the opportunity for accelerating ions to diffuse inward through the oxide scale [33]. Other observations on the harmful effects of Ta were also presented by Zhang [34] and Cui [35], but the detailed mechanism was not clarified. Additionally, the effects of multiple oxidation products containing Ta oxides on hot corrosion remained unclear.

Since preoxidation has been proven a promising method to retard the corrosion of superalloys, the stability of the preformed oxide scale on the surface of superalloys becomes crucial. In the present work, the 2nd generation SC superalloy N5 (containing 6.5 wt% Ta) was preoxidized under various designed conditions. Then, the N5 alloy with and without preoxidation was examined by the designed hot corrosion test. Since the molten sulfate is a typical type of molten salt deposit resulting from the fuel impurities, a systematic hot corrosion test was performed in mixed molten salts of 75 wt%  $\text{Na}_2\text{SO}_4$  + 25 wt%  $\text{K}_2\text{SO}_4$  at 850 °C. The influence of preoxidation on the hot corrosion behavior of the alloys was investigated. In particular, the role of Ta in the hot corrosion behavior of the substrate alloy and the superalloys with different preoxidation treatments was discussed in detail.

## 2. Experiment

### 2.1. Sample preparation

Cylindrical specimens of  $\Phi 15.0 \times 2.0$  mm were cut by electro spark wire cutting from the 2nd generation SC Ni-based superalloy N5 rods (produced by Institute of Metal Research, Chinese Academy of Sciences, Shenyang, China). The macroscopic morphologies and nominal chemical composition of the original specimens are shown in Fig. 1. The surfaces of these specimens were ground down to #600 metallographic SiC paper, and all the samples were chamfered by #600 metallographic SiC paper to make the edges and corners smooth. Any instability that the sharp corners would bring is avoided [31]. Then, the specimens were degreased by ultrasonically cleaning in a mixed solution of ethanol and

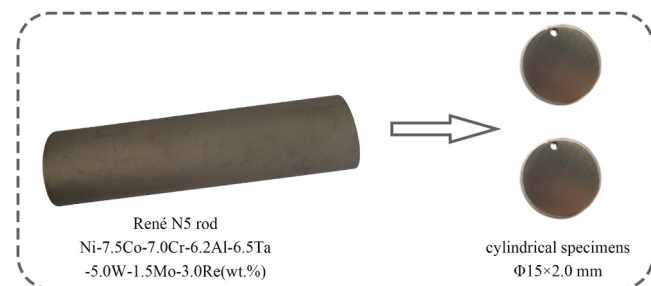


Fig. 1. Macroscopic morphologies of the single crystal superalloy René N5.

acetone (both analytical reagents, AR) (ratio of 3:1 in mass fraction), followed by drying with flowing cool air before the corrosion test.

### 2.2. Preoxidation treatment

Since the constituent and thickness of the surface oxide layer play a deciding role in the hot corrosion behavior of the alloy, different surface preoxidation treatments were carried out. According to our previous research and other reports about the oxidation regime of N5 alloy or any other superalloys that has a similar composition, relatively stable oxides could form on the surface of the alloy when oxidized at a temperature above 900 °C, and the oxide scale formed on the surface of the alloy when oxidized above 1100 °C could easily become unstable. Besides, as for the oxidation periods, oxidation of this alloy tended to enter the parabolic stage after 20 h, which meant the oxidation rate could keep relatively steady. As the oxidation temperature and periods increased, the oxide scale grew thicker and finally exfoliated after long-term oxidation [23–25,27,36]. In this work, preoxidation treatments were conducted in an air furnace that had already been heated at 900 °C, 1000 °C and 1100 °C, respectively. The preoxidation duration was set for 20 h and 100 h. After that, the oxidized specimens were removed from the furnace and cooled at room temperature. For keeping dry, the specimens were stocked in the desiccator for subsequent tests. According to different preoxidation temperatures, the specimens were classified into four groups: "0" (substrate), "1" (900 °C), "2" (1000 °C) and "3" (1100 °C). Because of the two preoxidation times at each temperature, all the specimens with different preoxidation treatments were presented as follows:  $0^{\text{sub}}$ ,  $1^{20\text{ h}}$ ,  $1^{100\text{ h}}$ ,  $2^{20\text{ h}}$ ,  $2^{100\text{ h}}$ ,  $3^{20\text{ h}}$ , and  $3^{100\text{ h}}$ , which are listed in Table 1.

### 2.3. Hot corrosion test

To simulate the real corrosive conditions, the method of precoating salt film was utilized in this experiment, which was first introduced by Simmons in the 1950 s [37] and has become a feasible and widely used method through constant modification in the laboratory test [14–18,38,39]. For the specific procedures, firstly, the specimens were preheated to 200 °C on a hot plate so that the salt layer could adhere well to the specimen surface. Then, the specimens were hand brushed with an oversaturated solution of a mixture of 75 wt%  $\text{Na}_2\text{SO}_4$  (AR) + 25 wt%  $\text{K}_2\text{SO}_4$  (AR) to obtain a solid membrane of deposit salt on the surface. The amount of the deposited solid salt was controlled by a mass range within  $2.0 \pm 0.2 \text{ mg/cm}^2$ . The salt brushing was kept at a suitable distance from the suspending hole of the specimen to avoid corrosion in this area. Secondly, the specimens coated with salt were suspended on a

**Table 1**  
Classification of the specimens under various pre-oxidation conditions.

Preoxidation	0	1	1	2	2	3	3
Temperature(°C)	-	900	900	1000	1000	1100	1100
Time(h)	-	20	100	20	100	20	100
Symbol	$0^{\text{sub}}$	$1^{20\text{ h}}$	$1^{100\text{ h}}$	$2^{20\text{ h}}$	$2^{100\text{ h}}$	$3^{20\text{ h}}$	$3^{100\text{ h}}$

Ni-Cr alloy frame and placed in a muffle furnace at 850 °C. The selection and determination of the temperature of hot corrosion are based on the mass ratio of the two mixed salts, and 850 °C is the state where the mixed salt film is in molten salt, and the corrosion is most severe. To be noticed, the amount of salt deposition in every cycle was indeed not much ( $2 \text{ mg/cm}^2$ ), the salt deposition just existed in a form of a thin layer of salt film. So, the molten salt film would not drop from the alloy surface. In fact, because of gravity, the molten salt would more or less downflow to make the bottom area of the samples suffer more serious corrosion. Thirdly, after a certain time, the corroded specimens were removed from the furnace and cooled in the air to room temperature. When the specimens were removed and cooled, the specimens were washed with boiling distilled water to remove the remnants of salts on the surfaces until the final distilled water was colorless and transparent. Finally, the washed specimens were dried with flowing cool air and weighed by using an electronic analytical balance (0.01 mg precision). After that, the specimens were rebrushed with the salts, and returned to the furnace by repeating the above procedures, forming a new cycle. The salt deposition was precisely controlled in the same amount in every cycle to reduce the experimental error. A total of ten cycles were conducted with a reaction time of 5 h in each cycle for the first eight cycles and 10 h reaction time for the last two cycles, leading to a total reaction time of 60 h. To reduce the experimental error caused by weight measurements, the average mass change of three parallel specimens in each group was adopted.

#### 2.4. Characterization methods

The preparation of the salt deposition and the mass change of the specimens were measured by an electronic analytical balance (0.01 mg precision, Sartorius SQP). X-ray diffraction was used to analyze the corrosion products of the specimens (X'Pert PRO, PANalytical Co., Almelo, Holland, Cu K $\alpha$  radiation at 40 kV). The phase constituent of the thin scale formed on specimens after preoxidation was characterized by grazing incidence X-ray diffraction (GI-XRD). Scanning electron microscopy (SEM, Inspect F50, FEI Co., Hillsboro, Oregon) equipped with energy dispersive spectroscopy (EDS, X-Max, Oxford Instruments Co., Oxford, UK) was used to examine the surface and cross-sectional morphology. Electron probe microanalysis (EPMA) was used to determine the distribution of elements and identify the corrosion products (JXA-8530 F, JEOL, Tokyo, Japan). For specimen protection and observation, a method of chemical Ni plating was employed for the surface of the cross-sectional specimens before the analysis.

### 3. Results

#### 3.1. Preoxidation products

**Fig. 2** shows the GI-XRD patterns of the preoxidized specimens. In addition to the alloy phases of  $\gamma/\gamma'$ , products of NiO,  $\alpha\text{-Al}_2\text{O}_3$  and Ta oxides were present for all the specimens.  $\text{NiAl}_2\text{O}_4$  was detected on the surface of all samples but not for  $1^{20\text{ h}}$ . With increasing preoxidation time and temperature, the intensity of  $\text{NiAl}_2\text{O}_4$  peaks became stronger. As the preoxidized temperature increased to 1100 °C ( $3^{20\text{ h}}$  and  $3^{100\text{ h}}$ ),  $\text{NiAl}_2\text{O}_4$  and  $\text{TaO}_x$  ( $x = 2$  or 2.5) dominated among the oxide products. These results are summarized in **Table 2**.

**Fig. 3** shows the cross-sectional morphologies of the specimens after preoxidation. In all cases, oxide scales were composed of multiple layers. However, the constituents and the thickness of the oxide scales were different. Combined our previous results [27] with those of others [23–26], it was found that the scales forming on  $1^{20\text{ h}}$  and  $1^{100\text{ h}}$  were thin and consisted of an inner continuous layer of  $\text{Al}_2\text{O}_3$  and an outer layer of NiO. The thickness of the scale on  $1^{20\text{ h}}$  was even less than 1  $\mu\text{m}$ . Compared with the results after preoxidation at 900 °C, the oxide scale by 1000 °C oxidation was with three layers in which an intermediate layer was found between the inner  $\text{Al}_2\text{O}_3$ - and the outer NiO-layers. The

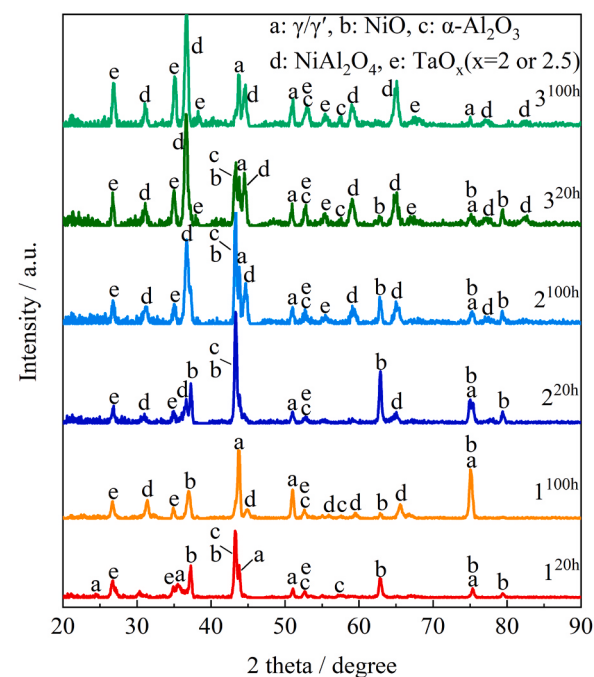


**Fig. 2.** XRD patterns of the specimens after preoxidation.

**Table 2**

XRD results of the specimens after different preoxidation condition and hot corrosion for 60 h.

Temperature (°C)/ Time (h)	Identified phases after preoxidation	Identified phases after hot corrosion for 60 h
- ( $0^{\text{sub}}$ )	-	NiO, $\text{NaTaO}_3$
900 / 20 ( $1^{20\text{ h}}$ )	NiO, $\alpha\text{-Al}_2\text{O}_3$ , $\text{TaO}_x$	NiO, $\alpha\text{-Al}_2\text{O}_3$ , $\text{Ni(Al, Cr)}_2\text{O}_4$
900 / 100 ( $1^{100\text{ h}}$ )	NiO, $\alpha\text{-Al}_2\text{O}_3$ , $\text{TaO}_x$ , $\text{NiAl}_2\text{O}_4$	NiO, $\alpha\text{-Al}_2\text{O}_3$ , $\text{Ni(Al, Cr)}_2\text{O}_4$
1000 / 20 ( $2^{20\text{ h}}$ )	NiO, $\alpha\text{-Al}_2\text{O}_3$ , $\text{TaO}_x$ , $\text{NiAl}_2\text{O}_4$	NiO, $\alpha\text{-Al}_2\text{O}_3$ , $\text{Ni(Al, Cr)}_2\text{O}_4$ , $\text{NaTaO}_3$
1000 / 100 ( $2^{100\text{ h}}$ )	NiO, $\alpha\text{-Al}_2\text{O}_3$ , $\text{TaO}_x$ , $\text{NiAl}_2\text{O}_4$	NiO, $\alpha\text{-Al}_2\text{O}_3$ , $\text{Ni(Al, Cr)}_2\text{O}_4$ , $\text{NaTaO}_3$
1100 / 20 ( $3^{20\text{ h}}$ )	NiO, $\alpha\text{-Al}_2\text{O}_3$ , $\text{TaO}_x$ , $\text{NiAl}_2\text{O}_4$	NiO, $\text{NaTaO}_3$ , $\text{Ni(Al, Cr)}_2\text{O}_4$
1100 / 10 ( $3^{100\text{ h}}$ )	NiO, $\alpha\text{-Al}_2\text{O}_3$ , $\text{TaO}_x$ , $\text{NiAl}_2\text{O}_4$	NiO, $\text{NaTaO}_3$ , $\text{Ni(Al, Cr)}_2\text{O}_4$

EDS results of the marked “1” in the intermediate layer of **Fig. 3(c)** showed 21.1 wt% Al, 7.0 wt% Cr, 23.0 wt% Ni and the rest of oxygen, indicating the formation of Ni-Al/Cr spinel. This three-layered structure was still observed for the oxidized specimen at 1100 °C after 20 h reaction, but when the reaction time reached 100 h, the scale consisted of an inner layer of  $\text{Al}_2\text{O}_3$  and an outer layer of  $\text{Ni(Al, Cr)}_2\text{O}_4$ . In addition, white and bright phases of Ta oxides appeared within the scale of all groups, in particular inside the  $\text{Ni(Al, Cr)}_2\text{O}_4$  intermediate layer. Ta oxides became more obvious as the preoxidized temperature and time increased. The thickness of the oxide scale increased from about 1.8  $\mu\text{m}$  at 900 °C to about 3.6  $\mu\text{m}$  at 1000 °C for 100 h, but no further significant increase was observed when the temperature increased to 1100 °C (**Fig. 3**).

#### 3.2. Hot corrosion

##### 3.2.1. Corrosion kinetics and surface appearance

**Fig. 4** shows the corrosion kinetics of the tested specimens. As shown in **Figs. 4(a)**, for  $2^{100\text{ h}}$ ,  $3^{20\text{ h}}$  and  $3^{100\text{ h}}$ , an obvious mass gain of up to 0.50  $\text{mg/cm}^2$  was observed at the early stage for 5 h, followed by a mass loss associated with the scale spallation and dissolution into the molten

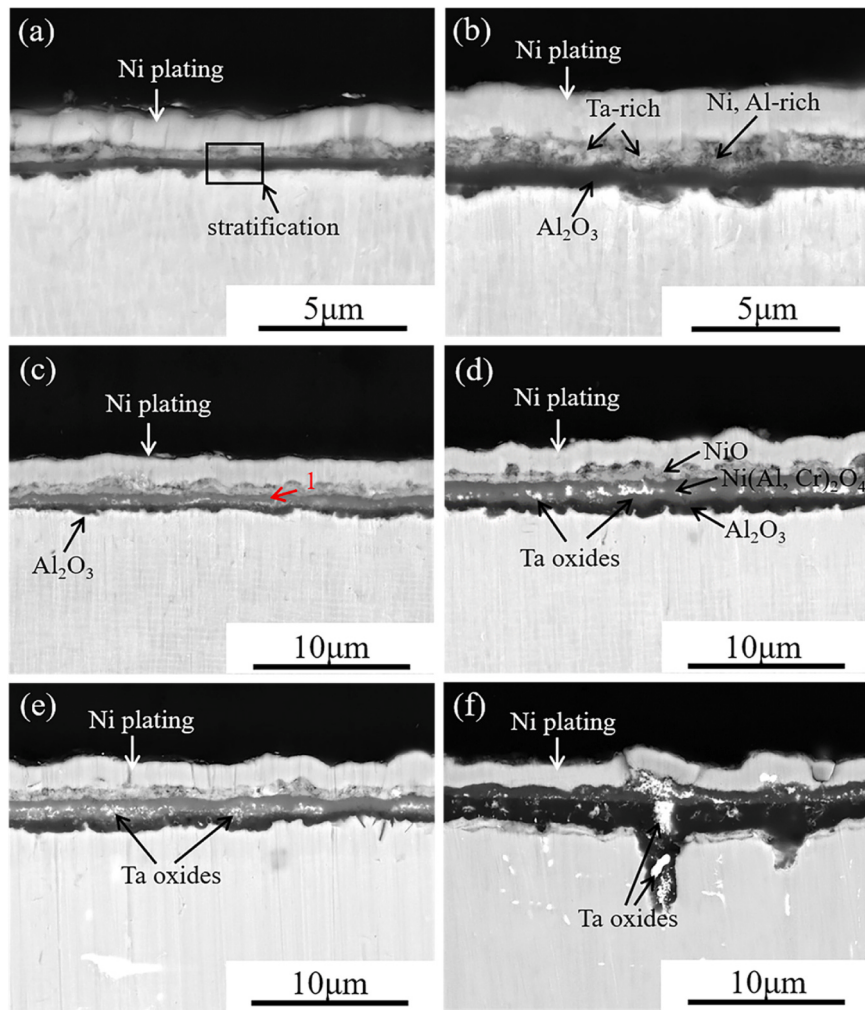


**Fig. 3.** Cross-sections of the specimens after preoxidation: (a)  $1^{20\text{ h}}$ , (b)  $1^{100\text{ h}}$ , (c)  $2^{20\text{ h}}$ , (d)  $2^{100\text{ h}}$ , (e)  $3^{20\text{ h}}$ , (f)  $3^{100\text{ h}}$ .

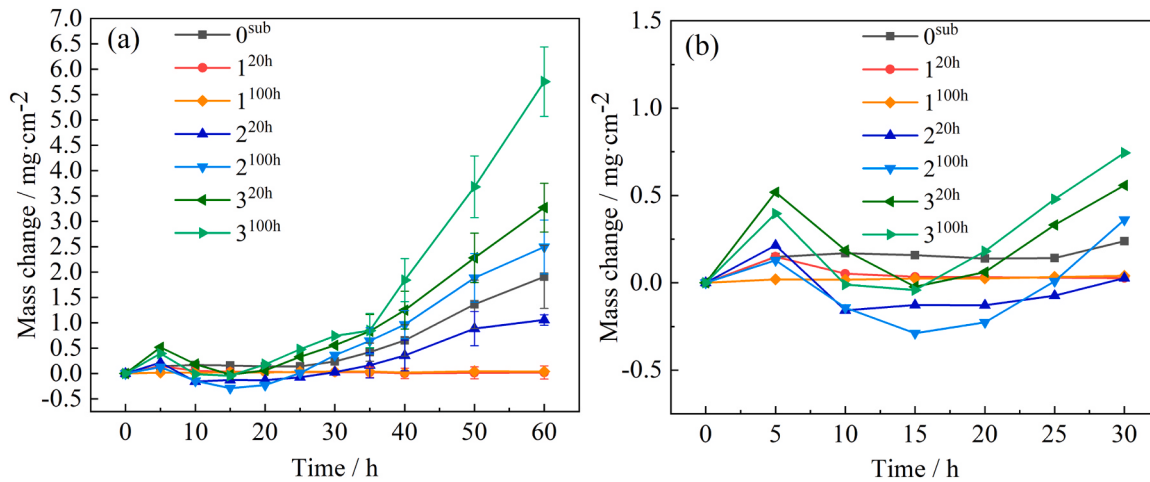


**Fig. 4.** Corrosion kinetics of the specimens under various preoxidation conditions in 75 wt%  $\text{Na}_2\text{SO}_4$  + 25 wt%  $\text{K}_2\text{SO}_4$  molten salts at 850 °C: (a) 60 h; (b) 30 h.

salts. After 15 h, the corrosion curves of these three groups of specimens showed a sharp increase in mass to the maximum reaction time of 60 h, which suggests that these three specimens suffered severe hot corrosion attack. The curve of  $2^{20\text{ h}}$  showed a similar trend to that of  $2^{100\text{ h}}$  except that the mass gain was much smaller after 25 h reaction. However, the kinetics curve for  $0^{\text{sub}}$  without preoxidation exhibited a steady trend

with just a slight mass gain until 30 h, followed by a continuous increase at the subsequent stage. The final mass gain was smaller than that of  $2^{100\text{ h}}$ ,  $3^{20\text{ h}}$  or  $3^{100\text{ h}}$ , indicating that preoxidation of these three groups of specimens accelerates hot corrosion attack. In contrast, there was almost no weight change recorded for  $1^{20\text{ h}}$  and  $1^{100\text{ h}}$  in the whole time period, indicating the best hot corrosion resistance.

Photographs of all the specimens after hot corrosion for 30 h and 60 h are shown in Fig. 5. This observation is basically in accordance with the phenomenon reflected by the corrosion kinetics shown in Fig. 4. It can be concluded that the specimens preoxidized at 1100 °C have suffered severe corrosion attack, while the specimens preoxidized at 900 °C indicated excellent corrosion resistance. For 0<sup>sub</sup>, the surface was rough with an obvious trace of corrosion after 30 h of reaction. In contrast, the scales of 1<sup>20h</sup> and 1<sup>100h</sup> were found to be compact and smooth after 60 h of corrosion. For 2<sup>20h</sup>, the 30 h surface appeared similar to 1<sup>20h</sup> and 1<sup>100h</sup>, but apparent corrosion was found as prolonged to 60 h. Differently, apparent corrosion occurred for 2<sup>100h</sup> after just 30 h because the scale became thick and loose. Severe corrosion deterioration with corner bulging occurred on the surfaces of both 3<sup>20h</sup> and 3<sup>100h</sup> after 30 h of corrosion. As the corrosion process proceeded, the bulge area on the surface extended and swelled, followed by visible spallation.

### 3.2.2. XRD patterns

Fig. 6 shows XRD patterns of the specimens exposed in 75 wt% Na<sub>2</sub>SO<sub>4</sub> + 25 wt% K<sub>2</sub>SO<sub>4</sub> molten salts at 850 °C for 60 h. XRD analysis confirms the presence of NiO and NaTaO<sub>3</sub> for 0<sup>sub</sup>. The products formed on 1<sup>20h</sup> and 1<sup>100h</sup> can be identified as NiO, α-Al<sub>2</sub>O<sub>3</sub> and Ni-Al/Cr spinels, but the NaTaO<sub>3</sub> phase was absent. The corrosion products for 2<sup>20h</sup>, 2<sup>100h</sup>, 3<sup>20h</sup> and 3<sup>100h</sup> were composed of NiO, Ni-Al/Cr spinels and NaTaO<sub>3</sub>, and α-Al<sub>2</sub>O<sub>3</sub> was also observed for 3<sup>20h</sup> and 3<sup>100h</sup>. These results are summarized in Table 2.

### 3.2.3. Surface morphologies

The surface observation was focused on the areas near the middle of the surface to avoid the bulges and spallation areas that appeared at the corners of some specimens. Fig. 7 shows the surface morphologies of the samples after corrosion for 60 h. For 0<sup>sub</sup> (Fig. 7(a)), the scale was mainly rich in Ni and Al by EDS analysis. The loose granular-like NiO scale was distributed on the surface. The scale of 1<sup>20h</sup> (Fig. 7(b)) was intact overall, and the outer surface was composed of NiO. Fig. 7(c) shows a complete and compact scale with good adhesion for 1<sup>100h</sup>. The EDS results indicated the presence of a (Ni, Al)-rich phase with some inner Al<sub>2</sub>O<sub>3</sub> particles distributed (inset in Fig. 7(c)). In addition, a small amount of white phase of Ta-rich oxides was also detected on the scale (Fig. 7c). The surface scale of 2<sup>20h</sup> (Fig. 7(d)) was similar to that of 1<sup>20h</sup> (Fig. 7(b)), except that the NiO particles became coarser and several pores/cracks appeared. In the case of 2<sup>100h</sup> (Fig. 7(e)), the scale was loose, and pores and cracks were observed on the surface. When the preoxidized temperature increased to 1100 °C, as shown in Fig. 7(f) and (g), the products were mainly composed of nonprotective NiO, and massive corrosion pores and spallation were observed on the surface, indicating that severe corrosion attack occurred.

### 3.2.4. Cross-sectional morphologies

The cross-sectional morphologies of all the groups after corrosion for 60 h are presented in Fig. 8. As shown in Fig. 8(a), the 0<sup>sub</sup> specimens were more severely corroded than the 1<sup>20h</sup> and 1<sup>100h</sup> specimens, forming a thicker scale. Pores and internal sulfides were found on the

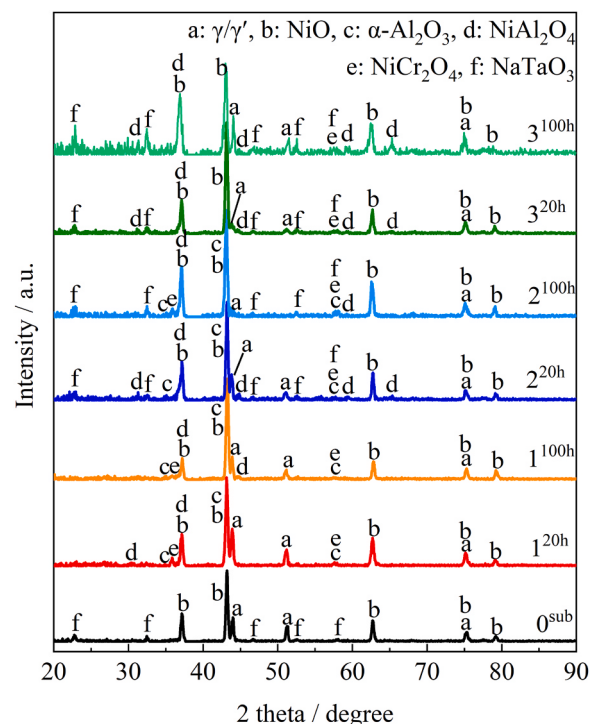


Fig. 6. XRD patterns of the specimens under various preoxidation conditions after hot corrosion at 850 °C in 75 wt% Na<sub>2</sub>SO<sub>4</sub> + 25 wt% K<sub>2</sub>SO<sub>4</sub> molten salts for 60 h.

scale and inside the matrix, respectively. The isolated dark particles (confirmed as CrS by EDS analysis) beneath the scale demonstrated that the penetration of S through the nonprotective scale reacted with the alloying element Cr after 60 h of corrosion. It is clearly indicated from the cross-section in Fig. 8(b) and (d) that the scales were complete and dense for 1<sup>20h</sup> and 1<sup>100h</sup>. The thickness and the oxide scale were almost the same as those of preoxidation before the corrosion test. The EDS analysis results of the points marked with "1", "2" and "3" in Fig. 8(b) are presented in Table 3. Combined with the EDS line scanning (Fig. 8(c)) along the arrow marked in Fig. 8(b), a three-layered structure can be identified, including an outer very thin NiO layer, a middle layer of Ni-Al/Cr spinel and an inner continuous Al<sub>2</sub>O<sub>3</sub>-rich layer formed on 1<sup>20h</sup> specimen. A small number of sulfidation particles was also found to disperse in the Al-depleted area (Fig. 8(b)). A similar structure was observed for 1<sup>100h</sup> sample with an increased thickness of the scale (Fig. 8d). The area mapping of this sample was done by EPMA and is shown in Fig. 9. An inner continuous protective Al<sub>2</sub>O<sub>3</sub> was formed inferred by the strong signals of Al and O, beneath which a thin Al-depleted zone was found. The S signal was detected in the area which corresponds well to the Al-depleted zone, forming a thin internal sulfidation layer beneath Al<sub>2</sub>O<sub>3</sub> (Fig. 8(d)). There was a clear Cr enrichment

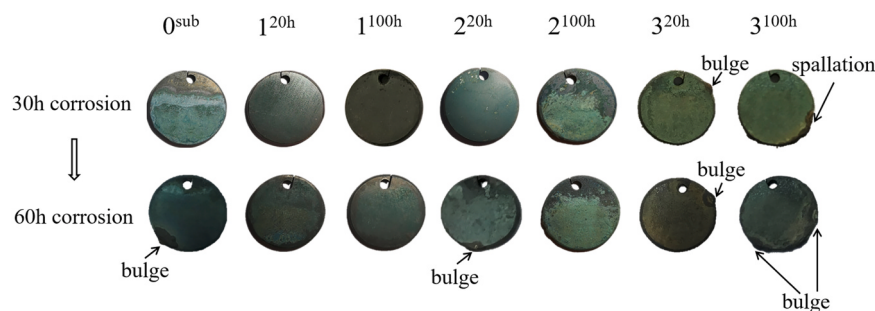
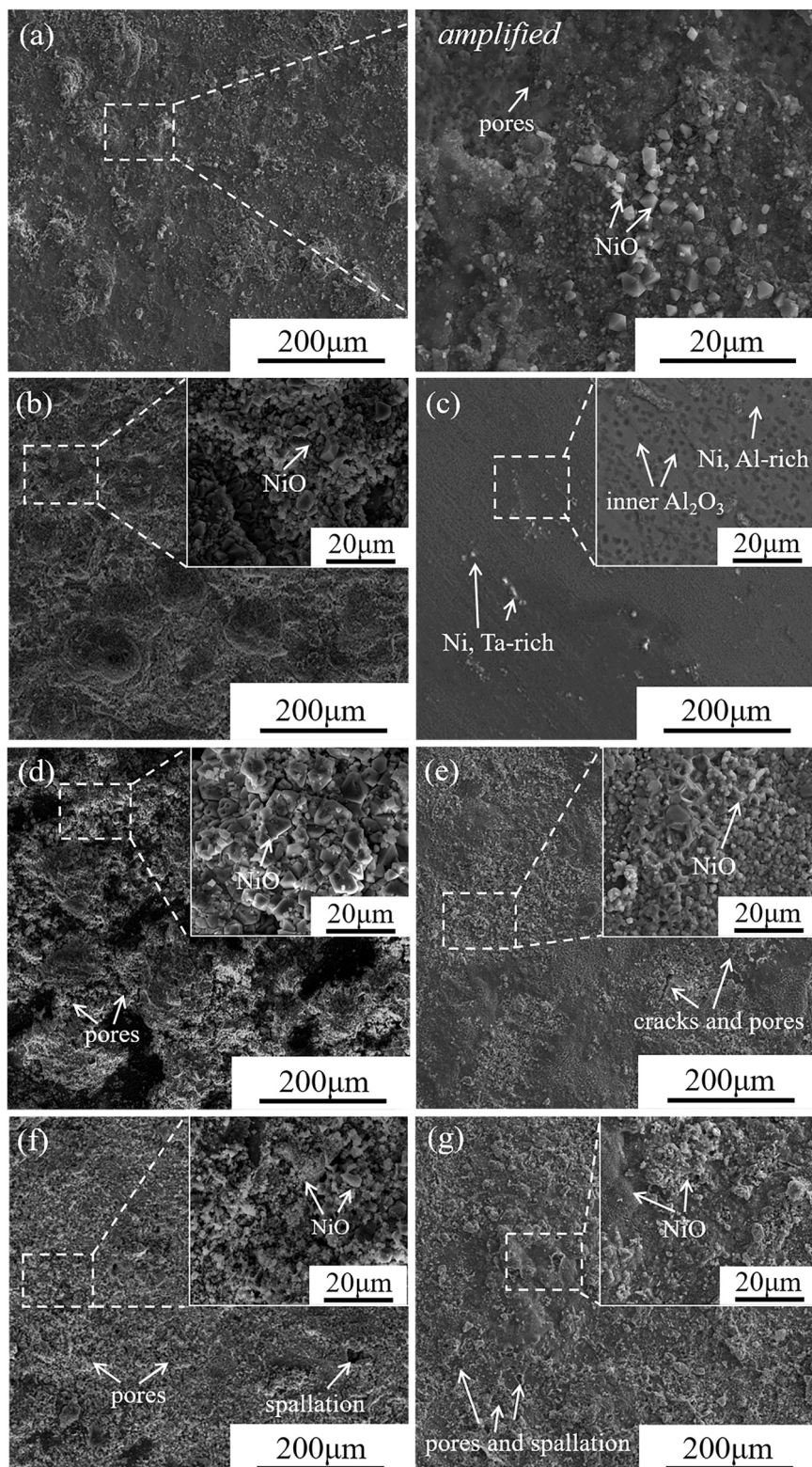


Fig. 5. Macrographs of the specimens under various preoxidation conditions after hot corrosion at 850 °C.



**Fig. 7.** Surface morphologies of the specimens after hot corrosion at 850 °C in 75 wt%  $\text{Na}_2\text{SO}_4$  + 25 wt%  $\text{K}_2\text{SO}_4$  molten salts for 60 h: (a)  $0^{\text{sub}}$ , (b)  $1^{20\text{ h}}$ , (c)  $1^{100\text{ h}}$ , (d)  $2^{20\text{ h}}$ , (e)  $2^{100\text{ h}}$ , (f)  $3^{20\text{ h}}$ , (g)  $3^{100\text{ h}}$ .

just above the  $\text{Al}_2\text{O}_3$  layer. No apparent Ta and W accumulation was found in the whole cross-section.

For  $2^{20\text{ h}}$  (Fig. 8(e)), the oxide scale was overall intact, and mainly composed of  $\text{Ni}(\text{Al}, \text{Cr})_2\text{O}_4$  as the EDS analysis results of the point marked with “4” shown in Table 3. However, a rough and loose scale and Ta-rich areas were clearly seen beneath the scale for  $2^{100\text{ h}}$  (Fig. 8(f)). In

addition, severe internal corrosion occurred with the presence of black  $\text{CrS}$  particles and white needle tantalum sulfides. When the preoxidized temperature increased to 1100 °C ( $3^{20\text{ h}}$  and  $3^{100\text{ h}}$  shown in Fig. 8(g) and (h)), the internal corrosion areas expanded to nearly 50  $\mu\text{m}$  deeper into the substrate. Many pores and cracks appeared on the surface scale with a large amount of tantalum oxides spreading nearby. Fig. 10 shows

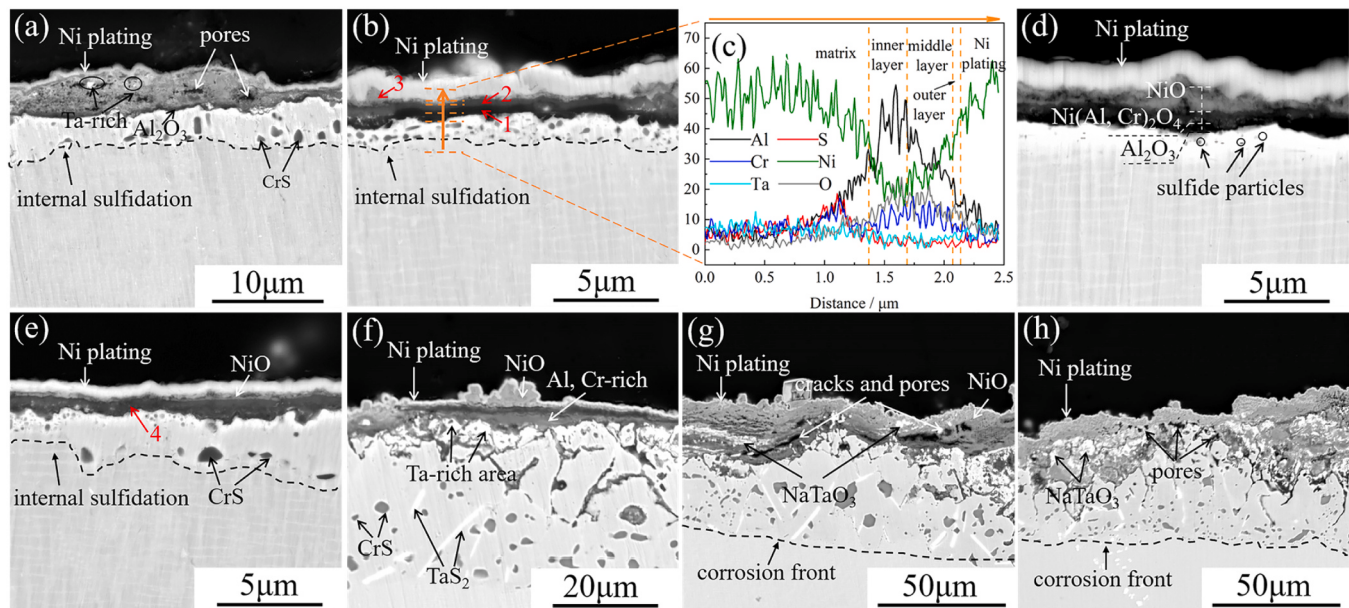


**Fig. 8.** Cross-sectional morphologies of the specimens after hot corrosion at 850 °C in 75 wt%  $\text{Na}_2\text{SO}_4$  + 25 wt%  $\text{K}_2\text{SO}_4$  molten salts for 60 h: (a)  $0^{\text{sub}}$ , (b)  $1^{20\text{ h}}$ , (c) EDS scanning along the orange line in (b), (d)  $1^{100\text{ h}}$ , (e)  $2^{20\text{ h}}$ , (f)  $2^{100\text{ h}}$ , (g)  $3^{20\text{ h}}$ , (h)  $3^{100\text{ h}}$ .

**Table 3**

EDS results of the marked points in Fig. 8 (wt%).

Elements	Al	S	Cr	Ni	Ta	Co	Na	O
1	33.1	1.8	3.8	6.2	2.6	1.0	-	51.5
2	23.0	0.2	6.3	17.0	1.4	2.8	-	49.3
3	9.8	1.0	2.8	52.3	1.7	1.8	0.1	30.5
4	17.5	0.6	6.2	27	8.2	2.0	0.3	38.2

an area mapping by EPMA for  $3^{100\text{ h}}$  after corrosion for 60 h. There was an enrichment of Ni on the surface of the scale but no continuous  $\text{Al}_2\text{O}_3$  layer. Elements of Al, Ta and Cr were enriched inside the scale but distributed nonuniformly. More CrS particles were found under the scale as revealed by both Cr and S maps (Fig. 10).

#### 4. Discussion

The difference of the tested specimens is that they experienced different preoxidation before hot corrosion. The structure and composition of the oxide scales formed on the surfaces of the specimens after preoxidation varied with the oxidizing temperature and time, leading to different performances of these specimens when exposed to a hot

corrosive environment in 75 wt%  $\text{Na}_2\text{SO}_4$  + 25 wt%  $\text{K}_2\text{SO}_4$  molten salts at 850 °C. Clearly, the preformed oxide scale plays an effect on hot corrosion by interaction with the base alloy underneath and the molten salt on the top. The discussion will first go to the effect of temperature on preoxidized scale formation, and then understand the role of this preformed oxide scale on hot corrosion by interaction with the salt and the alloy. The effect of Ta on hot corrosion will also be discussed.

#### 4.1. Preoxide scale formation

As revealed by Figs. 2 and 3, pre-oxidation led to the formation of an oxide scale. In general, this oxide scale contained three layers of top NiO and bottom  $\text{Al}_2\text{O}_3$  layers together with a  $\text{Ni}(\text{Al}, \text{Cr})_2\text{O}_4$  layer in between. In addition, Ta-rich oxides were found inside the scale. The thicknesses of these oxide layers and the amount of Ta-rich oxides varied with the temperature and the reaction time. At a low temperature, 900 °C, a thin oxide scale was formed where a thin but continuous alumina layer was observed. At this temperature, much less  $\text{NiAl}_2\text{O}_4$  and Ta-rich oxide were detected (Fig. 2 and Table 2). Increasing the temperature to 1000 °C and further to 1100 °C increased the total thickness of the scale where both alumina and  $\text{Ni}(\text{Al}, \text{Cr})_2\text{O}_4$  layers were thickened but NiO layer became thinner (Fig. 3). More Ta-rich oxides were identified with

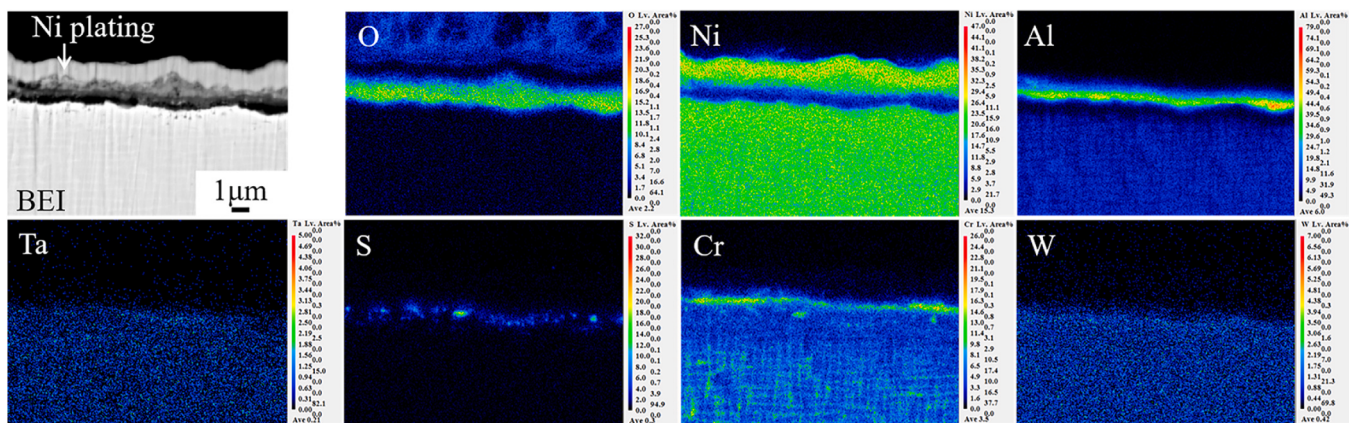


**Fig. 9.** EPMA maps of the  $1^{100\text{ h}}$  after corrosion at 850 °C in 75 wt%  $\text{Na}_2\text{SO}_4$  + 25 wt%  $\text{K}_2\text{SO}_4$  molten salts for 60 h.

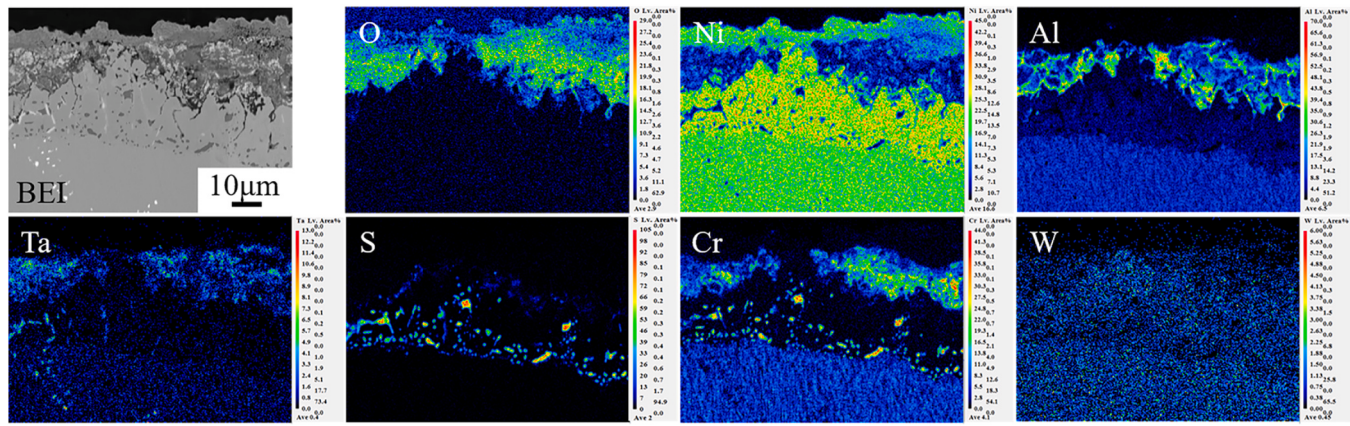


Fig. 10. EPMA maps of the 3<sup>100</sup> h after corrosion at 850 °C in 75 wt% Na<sub>2</sub>SO<sub>4</sub> + 25 wt% K<sub>2</sub>SO<sub>4</sub> molten salts for 60 h.

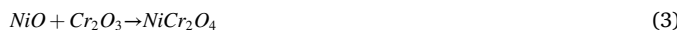
increasing temperature and reaction time. Clearly temperature and alloy composition play important roles in metal diffusion and therefore the reaction kinetics.

The observation of alumina layer formation in all conditions reveals that the critical concentration of Al for the conversion from internal oxidation to external oxidation has been reached. In addition, the accelerating effect of Cr on alumina formation has been reported extensively [18,40] which could also be the case for this particular alloy. The observation of Cr immediately on the top of alumina (Fig. 9) provides evidence of this effect where Cr plays a third element effect to lower the interface  $P_{O_2}$  value and therefore reduce oxygen solubility  $N_O$  at this interface. As a result, the critical Al concentration for alumina formation is reduced according to Wagner's equation [41,42] :

$$N_{Al(min)} = \left( \frac{3\pi g^* N_O D_O V_{Al}}{4D_{Al} V_{Ox}} \right)^{1/2} \quad (1)$$

where  $N_{Al(min)}$  is the critical Al content to form Al<sub>2</sub>O<sub>3</sub>,  $N_O D_O$  is the oxygen permeability,  $g^*$  is the factor depending on the volume fraction of Al<sub>2</sub>O<sub>3</sub> required for the formation of an external oxide scale,  $D_{Al}$  is the diffusion coefficient of Al in the alloy, and  $V_{Al}$  and  $V_{Ox}$  are the molar volumes of Al and Al<sub>2</sub>O<sub>3</sub> scale. When the content of Al in the alloy exceeds the critical content ( $N_{Al} \geq N_{Al(min)}$ ), a continuous and external Al<sub>2</sub>O<sub>3</sub> scale will form on the surface of the alloy.

The increased thickness of Ni(Al, Cr)<sub>2</sub>O<sub>4</sub> but decreased NiO thickness with increasing temperature can be understood by the accelerated Al outward diffusion and interaction with NiO according to the following reactions:



The formation of Ni(Al, Cr)<sub>2</sub>O<sub>4</sub> will consume NiO, and the observed increased Ni(Al, Cr)<sub>2</sub>O<sub>4</sub> thickness but decreased NiO thickness are explained. At 1100 °C for 100 h, almost all NiO has been converted to Ni(Al, Cr)<sub>2</sub>O<sub>4</sub> and therefore no NiO can be found in both XRD (Fig. 2, Table 2) and the cross-section (Fig. 3).

Ta-rich oxide formation was observed above the alumina layer and inside the middle layer of NiAl<sub>2</sub>O<sub>4</sub>. The location of this oxide is in agreement with its stability as shown in Fig. 11 where Ta<sub>2</sub>O<sub>5</sub> is less stable than Al<sub>2</sub>O<sub>3</sub>. Therefore, Ta<sub>2</sub>O<sub>5</sub> can only form in the place above the alumina layer where  $P_{O_2}$  is high to stabilize Ta<sub>2</sub>O<sub>5</sub>. Clearly, increasing temperature enhances the Ta<sub>2</sub>O<sub>5</sub> formation kinetics.

#### 4.2. Hot corrosion of alloy without pre-oxidation

Unlike isothermal oxidation in air, in molten sulfate corrosion, there exists a competition between the destructive spallation/dissolution and

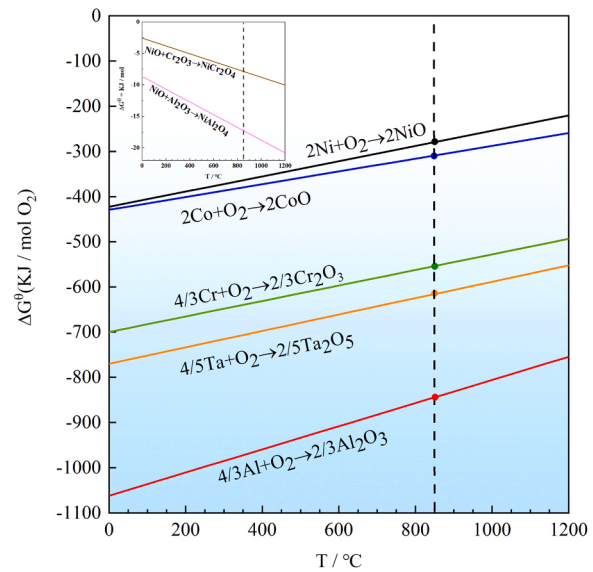
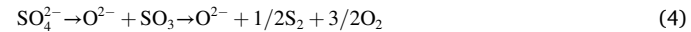


Fig. 11. Ellingham diagram for oxides of the alloying elements in the experimental alloy (The inset is for the Ni-Al/Cr spinel).

the reformation of the oxide scale, which results in different evolution stages of the scale [15,20]. For the original N5 alloy (0<sup>subb</sup>) without preoxidation, the alloy will react with the salts, forming oxides and sulfides. The molten sulfates can provide oxygen and sulfur for the below reactions as shown in Reaction (4) [6,10]:



As the activity of O<sup>2-</sup> at the alloy/salts interface increases, the scale dissolution occurred, following the basic fluxing, according to Reactions (5) and (6) [6,10]:



Both NiO<sub>2</sub><sup>2-</sup> and AlO<sub>2</sub><sup>-</sup> will diffuse from the alloy/salt interface to the salt/gas interface where these metallic oxide ions would decompose, forming loose metallic oxides due to the relatively low activity of O<sup>2-</sup> there. In the meantime, constant oxidation of the alloy leads to the O partial pressure reduction at the alloy/salt interface. As a result, the S partial pressure increases. As the oxide scale is porous, S could easily penetrate into the alloy to form the internal sulfides.

Based on the above discussion, the competition between the disso-

lution and the reformation of the oxide scale could be regarded as an important parameter to explain the corrosion process. Here, this competition could be simply represented by the overall mass change as follows:

$$\Delta M = M_{f/g} - M_{d/s} \quad (7)$$

$M_{f/g}$  and  $M_{d/s}$  represented the formation/growth and dissolution/spallation of the oxide scale, respectively. Table 4 shows the mass change in different corrosion stages.

For the corrosion process of  $0^{\text{sub}}$ , there are two major stages: an incubation period and a propagation period (Fig. 4(a)). In the incubation period (before 30 h),  $M_{f/g} \approx M_{d/s}$ ,  $\Delta M \approx 0$ . Initial rapid oxidation will be balanced by the dissolution of the scale. In addition, without previous consumption of Al, a thin  $\text{Al}_2\text{O}_3$  layer could form under the coverage of the sulfate salts and retard corrosion to some extent. Fig. 12(a) shows the cross-section of sample  $0^{\text{sub}}$  after hot corrosion for 30 h reaction. The formation of a rough scale surface indicates the occurrence of the oxide dissolution into the molten salt with just a very thin and discontinuous  $\text{Al}_2\text{O}_3$  layer at 30 h. After 30 h of corrosion, a continuous mass gain occurred, indicating the propagation period has started (Fig. 4(a)). The molten salt penetrated into the substrate, and obvious internal sulfidation occurred (Fig. 12(a)). Further increasing the reaction time to 60 h, no continuous  $\text{Al}_2\text{O}_3$  could form, and massive nonprotective oxides and corrosion pores were observed (Fig. 8(a)). As a result, significant corrosion degradation was developed.

#### 4.3. Effect of pre-oxidation on hot corrosion

In this work, preoxidation was found to play an important role in the hot corrosion described above. Samples of  $1^{20\text{ h}}$  and  $1^{100\text{ h}}$  ( $900^{\circ}\text{C}$  preoxidized) exhibited the best corrosion resistance, whose weight change kinetic curves remained with almost no change throughout the whole corrosion process (Fig. 4(a)). This means that the destruction and reformation of the oxide scale reaches a balance. Clearly, the preformed  $\text{Al}_2\text{O}_3$  and/or Ni-Al/Cr spinel (Fig. 8(d)) reduced the diffusion of oxygen and sulfur and therefore the corrosion rate. As demonstrated by the element mapping of this sample after  $900^{\circ}\text{C}$  preoxidation (Fig. 9), a thin continuous  $\text{Al}_2\text{O}_3$  layer with a shallow Al depletion zone was observed. Also, there was less internal oxidation and limited sulphidation (Fig. 9). Therefore, this sample has a strong tendency for repairing the alumina scale if any dissolution or damage of this scale occurs because of enough aluminum supply from the substrate to keep the competition in balance during continuous hot corrosion. Based on the above results, forming a protective oxide scale that is thick enough and retains the scale-forming elements as much as possible plays a decisive role in maintaining the hot corrosion resistance of the alloy.

It has been proven that NiO cannot effectively prevent the development of corrosion due to its loose and porous characteristics [12]. Singh et al. [43] reported that NiO provides worse hot corrosion resistance than  $\text{NiAl}_2\text{O}_4$  spinel since the solubility of  $\text{NiAl}_2\text{O}_4$  is thermodynamically lower than that of NiO in molten salts. Although  $\text{NiAl}_2\text{O}_4$  had an anti-corrosion ability to a certain extent, it was easier to spall and dissolve in the molten salts than  $\text{Al}_2\text{O}_3$ . Meanwhile, tremendous Al consumption

**Table 4**  
Different corrosion stages for all the tested specimens.

	$\Delta M = M_{f/g} - M_{d/s}$	$0^{\text{sub}}$	$1^{20\text{ h}}/1^{100\text{ h}}$	$2^{20\text{ h}}/2^{100\text{ h}}/3^{20\text{ h}}/3^{100\text{ h}}$
Incubation stage	$M_{f/g} \approx M_{d/s}$ , $\Delta M \approx 0$ (<30 h)	$M_{f/g} \approx M_{d/s}$ , $\Delta M \approx 0$	-	-
Unstable stage	-	-	$M_{f/g} < M_{d/s}$ , $\Delta M < 0$ (<15 h)	-
Propagation stage	$M_{f/g} > M_{d/s}$ , $\Delta M > 0$ (>30 h)	-	$M_{f/g} > M_{d/s}$ , $\Delta M > 0$ (>15 h)	-

during higher temperature preoxidation e.g.  $1000^{\circ}\text{C}$  and  $1100^{\circ}\text{C}$  in this work led to a situation in which the Al content was not sufficient to constantly produce a continuous scale of  $\text{Al}_2\text{O}_3$  as the subsequent corrosion process proceeded. Once a dense and continuous layer of protective  $\text{Al}_2\text{O}_3$  could not form, the surface scale lost protectiveness. As a result, scale dissolution dominated, and mass loss occurred.

Corrosion degradation occurred for specimens preoxidized at  $1000^{\circ}\text{C}$  and  $1100^{\circ}\text{C}$  ( $2^{20\text{ h}}/3^{100\text{ h}}$ ), as shown in the kinetics curves (Fig. 4(b)). All specimens showed a trend of continuous mass loss from 5 to 15 h followed by a sharp continuous mass gain after 15 h. In the incubation period (before 15 h),  $M_{f/g} < M_{d/s}$ ,  $\Delta M < 0$ . The preformed oxide scales presented a multilayer structure mainly composed of NiO, Ni(Al, Cr) $_2\text{O}_4$  and  $\text{Al}_2\text{O}_3$ , as shown in Fig. 3. In the propagation period (after 15 h),  $M_{f/g} > M_{d/s}$ ,  $\Delta M > 0$ . Hot corrosion is a rapid and violent redox reaction. Although continuous protective  $\text{Al}_2\text{O}_3$  was no longer able to form, the oxidation reaction of other alloying elements occurred constantly. The corrosion scales of  $3^{20\text{ h}}$  and  $3^{100\text{ h}}$  (Fig. 12(g) and (h)) had rupture characteristics, and notable corrosion pores and penetrating cracks appeared. The outward diffusion to the scale/substrate interface of Ni, Cr and Co resulted in the formation of related nonprotective oxides. From reaction (4), the constant consumption of O will result in an increase in the S partial pressure, and therefore the formation of internal sulfides. Many isolated dark particles detected as CrS were observed in Fig. 8(f)-(h). This phenomenon was due to the fact that S in the molten salt penetrated inward into the substrate through the scale and reacted mainly with Cr to form CrS [17,44]. Once the molten salts penetrated the scale to form the internal sulfides, cracks and pores would be produced in/beneath the scale, thereby accelerating hot corrosion. Therefore, the amount and depth of internal sulfides could reflect the degree of hot corrosion to a certain extent. As the oxide scales were dissolved into the molten salts by the basic fluxing (reactions (4)-(6)), the metallic oxide ions would decompose, and loose metallic oxides would precipitate at the salt/gas interface as discussed in Section 4.2. This process tended to take precedence where pitting occurred. The local defects, such as bulges in the pitting place, became larger over time, which makes it clear that there was a continuous mass gain in the propagation stage. Less Ta oxide distribution in the scale reduced the adverse Ta effect on the corrosion behavior, which will be discussed in the next Section 4.4.

#### 4.4. Ta effect on hot corrosion

Ta is a refractory alloying element used to improve the high-temperature mechanical properties of nickel-based superalloys. However, excessive Ta may have adverse effects on the corrosion properties of superalloys. During the preoxidation process, Ta oxides became more obvious as the preoxidized temperature and time increased. Especially for the  $3^{100\text{ h}}$  group preoxidized at  $1100^{\circ}\text{C}$  for 100 h (Fig. 3(f)), massive white phases of Ta oxides had already distributed in the oxide scale after preoxidation, resulting in severe defects on the oxide scale during the corrosion test. Based on the Ellingham diagram in Fig. 11, Ta had a strong affinity with O because the standard free energy of its oxide was lower than that of the other alloying elements apart from Al. A large amount of  $\text{Ta}_2\text{O}_5$  is segregated in the oxide scale. Since the coefficient of thermal expansion (CTE) of  $\text{Ta}_2\text{O}_5$  is  $4 \times 10^{-6}$  at  $550\text{--}1200^{\circ}\text{C}$ , which is much lower than that of  $\text{Al}_2\text{O}_3$  ( $8.1 \times 10^{-6}\text{--}10^{-5}\text{--}10^{-4}\text{--}10^{-3}\text{--}10^{-2}\text{--}10^{-1}\text{--}10^{-2}\text{--}10^{-3}\text{--}10^{-4}\text{--}10^{-5}\text{--}10^{-6}\text{--}10^{-7}\text{--}10^{-8}\text{--}10^{-9}\text{--}10^{-10}\text{--}10^{-11}\text{--}10^{-12}\text{--}10^{-13}\text{--}10^{-14}\text{--}10^{-15}\text{--}10^{-16}\text{--}10^{-17}\text{--}10^{-18}\text{--}10^{-19}\text{--}10^{-20}\text{--}10^{-21}\text{--}10^{-22}\text{--}10^{-23}\text{--}10^{-24}\text{--}10^{-25}\text{--}10^{-26}\text{--}10^{-27}\text{--}10^{-28}\text{--}10^{-29}\text{--}10^{-30}\text{--}10^{-31}\text{--}10^{-32}\text{--}10^{-33}\text{--}10^{-34}\text{--}10^{-35}\text{--}10^{-36}\text{--}10^{-37}\text{--}10^{-38}\text{--}10^{-39}\text{--}10^{-40}\text{--}10^{-41}\text{--}10^{-42}\text{--}10^{-43}\text{--}10^{-44}\text{--}10^{-45}\text{--}10^{-46}\text{--}10^{-47}\text{--}10^{-48}\text{--}10^{-49}\text{--}10^{-50}\text{--}10^{-51}\text{--}10^{-52}\text{--}10^{-53}\text{--}10^{-54}\text{--}10^{-55}\text{--}10^{-56}\text{--}10^{-57}\text{--}10^{-58}\text{--}10^{-59}\text{--}10^{-60}\text{--}10^{-61}\text{--}10^{-62}\text{--}10^{-63}\text{--}10^{-64}\text{--}10^{-65}\text{--}10^{-66}\text{--}10^{-67}\text{--}10^{-68}\text{--}10^{-69}\text{--}10^{-70}\text{--}10^{-71}\text{--}10^{-72}\text{--}10^{-73}\text{--}10^{-74}\text{--}10^{-75}\text{--}10^{-76}\text{--}10^{-77}\text{--}10^{-78}\text{--}10^{-79}\text{--}10^{-80}\text{--}10^{-81}\text{--}10^{-82}\text{--}10^{-83}\text{--}10^{-84}\text{--}10^{-85}\text{--}10^{-86}\text{--}10^{-87}\text{--}10^{-88}\text{--}10^{-89}\text{--}10^{-90}\text{--}10^{-91}\text{--}10^{-92}\text{--}10^{-93}\text{--}10^{-94}\text{--}10^{-95}\text{--}10^{-96}\text{--}10^{-97}\text{--}10^{-98}\text{--}10^{-99}\text{--}10^{-100}\text{--}10^{-101}\text{--}10^{-102}\text{--}10^{-103}\text{--}10^{-104}\text{--}10^{-105}\text{--}10^{-106}\text{--}10^{-107}\text{--}10^{-108}\text{--}10^{-109}\text{--}10^{-110}\text{--}10^{-111}\text{--}10^{-112}\text{--}10^{-113}\text{--}10^{-114}\text{--}10^{-115}\text{--}10^{-116}\text{--}10^{-117}\text{--}10^{-118}\text{--}10^{-119}\text{--}10^{-120}\text{--}10^{-121}\text{--}10^{-122}\text{--}10^{-123}\text{--}10^{-124}\text{--}10^{-125}\text{--}10^{-126}\text{--}10^{-127}\text{--}10^{-128}\text{--}10^{-129}\text{--}10^{-130}\text{--}10^{-131}\text{--}10^{-132}\text{--}10^{-133}\text{--}10^{-134}\text{--}10^{-135}\text{--}10^{-136}\text{--}10^{-137}\text{--}10^{-138}\text{--}10^{-139}\text{--}10^{-140}\text{--}10^{-141}\text{--}10^{-142}\text{--}10^{-143}\text{--}10^{-144}\text{--}10^{-145}\text{--}10^{-146}\text{--}10^{-147}\text{--}10^{-148}\text{--}10^{-149}\text{--}10^{-150}\text{--}10^{-151}\text{--}10^{-152}\text{--}10^{-153}\text{--}10^{-154}\text{--}10^{-155}\text{--}10^{-156}\text{--}10^{-157}\text{--}10^{-158}\text{--}10^{-159}\text{--}10^{-160}\text{--}10^{-161}\text{--}10^{-162}\text{--}10^{-163}\text{--}10^{-164}\text{--}10^{-165}\text{--}10^{-166}\text{--}10^{-167}\text{--}10^{-168}\text{--}10^{-169}\text{--}10^{-170}\text{--}10^{-171}\text{--}10^{-172}\text{--}10^{-173}\text{--}10^{-174}\text{--}10^{-175}\text{--}10^{-176}\text{--}10^{-177}\text{--}10^{-178}\text{--}10^{-179}\text{--}10^{-180}\text{--}10^{-181}\text{--}10^{-182}\text{--}10^{-183}\text{--}10^{-184}\text{--}10^{-185}\text{--}10^{-186}\text{--}10^{-187}\text{--}10^{-188}\text{--}10^{-189}\text{--}10^{-190}\text{--}10^{-191}\text{--}10^{-192}\text{--}10^{-193}\text{--}10^{-194}\text{--}10^{-195}\text{--}10^{-196}\text{--}10^{-197}\text{--}10^{-198}\text{--}10^{-199}\text{--}10^{-200}\text{--}10^{-201}\text{--}10^{-202}\text{--}10^{-203}\text{--}10^{-204}\text{--}10^{-205}\text{--}10^{-206}\text{--}10^{-207}\text{--}10^{-208}\text{--}10^{-209}\text{--}10^{-210}\text{--}10^{-211}\text{--}10^{-212}\text{--}10^{-213}\text{--}10^{-214}\text{--}10^{-215}\text{--}10^{-216}\text{--}10^{-217}\text{--}10^{-218}\text{--}10^{-219}\text{--}10^{-220}\text{--}10^{-221}\text{--}10^{-222}\text{--}10^{-223}\text{--}10^{-224}\text{--}10^{-225}\text{--}10^{-226}\text{--}10^{-227}\text{--}10^{-228}\text{--}10^{-229}\text{--}10^{-230}\text{--}10^{-231}\text{--}10^{-232}\text{--}10^{-233}\text{--}10^{-234}\text{--}10^{-235}\text{--}10^{-236}\text{--}10^{-237}\text{--}10^{-238}\text{--}10^{-239}\text{--}10^{-240}\text{--}10^{-241}\text{--}10^{-242}\text{--}10^{-243}\text{--}10^{-244}\text{--}10^{-245}\text{--}10^{-246}\text{--}10^{-247}\text{--}10^{-248}\text{--}10^{-249}\text{--}10^{-250}\text{--}10^{-251}\text{--}10^{-252}\text{--}10^{-253}\text{--}10^{-254}\text{--}10^{-255}\text{--}10^{-256}\text{--}10^{-257}\text{--}10^{-258}\text{--}10^{-259}\text{--}10^{-260}\text{--}10^{-261}\text{--}10^{-262}\text{--}10^{-263}\text{--}10^{-264}\text{--}10^{-265}\text{--}10^{-266}\text{--}10^{-267}\text{--}10^{-268}\text{--}10^{-269}\text{--}10^{-270}\text{--}10^{-271}\text{--}10^{-272}\text{--}10^{-273}\text{--}10^{-274}\text{--}10^{-275}\text{--}10^{-276}\text{--}10^{-277}\text{--}10^{-278}\text{--}10^{-279}\text{--}10^{-280}\text{--}10^{-281}\text{--}10^{-282}\text{--}10^{-283}\text{--}10^{-284}\text{--}10^{-285}\text{--}10^{-286}\text{--}10^{-287}\text{--}10^{-288}\text{--}10^{-289}\text{--}10^{-290}\text{--}10^{-291}\text{--}10^{-292}\text{--}10^{-293}\text{--}10^{-294}\text{--}10^{-295}\text{--}10^{-296}\text{--}10^{-297}\text{--}10^{-298}\text{--}10^{-299}\text{--}10^{-300}\text{--}10^{-301}\text{--}10^{-302}\text{--}10^{-303}\text{--}10^{-304}\text{--}10^{-305}\text{--}10^{-306}\text{--}10^{-307}\text{--}10^{-308}\text{--}10^{-309}\text{--}10^{-310}\text{--}10^{-311}\text{--}10^{-312}\text{--}10^{-313}\text{--}10^{-314}\text{--}10^{-315}\text{--}10^{-316}\text{--}10^{-317}\text{--}10^{-318}\text{--}10^{-319}\text{--}10^{-320}\text{--}10^{-321}\text{--}10^{-322}\text{--}10^{-323}\text{--}10^{-324}\text{--}10^{-325}\text{--}10^{-326}\text{--}10^{-327}\text{--}10^{-328}\text{--}10^{-329}\text{--}10^{-330}\text{--}10^{-331}\text{--}10^{-332}\text{--}10^{-333}\text{--}10^{-334}\text{--}10^{-335}\text{--}10^{-336}\text{--}10^{-337}\text{--}10^{-338}\text{--}10^{-339}\text{--}10^{-340}\text{--}10^{-341}\text{--}10^{-342}\text{--}10^{-343}\text{--}10^{-344}\text{--}10^{-345}\text{--}10^{-346}\text{--}10^{-347}\text{--}10^{-348}\text{--}10^{-349}\text{--}10^{-350}\text{--}10^{-351}\text{--}10^{-352}\text{--}10^{-353}\text{--}10^{-354}\text{--}10^{-355}\text{--}10^{-356}\text{--}10^{-357}\text{--}10^{-358}\text{--}10^{-359}\text{--}10^{-360}\text{--}10^{-361}\text{--}10^{-362}\text{--}10^{-363}\text{--}10^{-364}\text{--}10^{-365}\text{--}10^{-366}\text{--}10^{-367}\text{--}10^{-368}\text{--}10^{-369}\text{--}10^{-370}\text{--}10^{-371}\text{--}10^{-372}\text{--}10^{-373}\text{--}10^{-374}\text{--}10^{-375}\text{--}10^{-376}\text{--}10^{-377}\text{--}10^{-378}\text{--}10^{-379}\text{--}10^{-380}\text{--}10^{-381}\text{--}10^{-382}\text{--}10^{-383}\text{--}10^{-384}\text{--}10^{-385}\text{--}10^{-386}\text{--}10^{-387}\text{--}10^{-388}\text{--}10^{-389}\text{--}10^{-390}\text{--}10^{-391}\text{--}10^{-392}\text{--}10^{-393}\text{--}10^{-394}\text{--}10^{-395}\text{--}10^{-396}\text{--}10^{-397}\text{--}10^{-398}\text{--}10^{-399}\text{--}10^{-400}\text{--}10^{-401}\text{--}10^{-402}\text{--}10^{-403}\text{--}10^{-404}\text{--}10^{-405}\text{--}10^{-406}\text{--}10^{-407}\text{--}10^{-408}\text{--}10^{-409}\text{--}10^{-410}\text{--}10^{-411}\text{--}10^{-412}\text{--}10^{-413}\text{--}10^{-414}\text{--}10^{-415}\text{--}10^{-416}\text{--}10^{-417}\text{--}10^{-418}\text{--}10^{-419}\text{--}10^{-420}\text{--}10^{-421}\text{--}10^{-422}\text{--}10^{-423}\text{--}10^{-424}\text{--}10^{-425}\text{--}10^{-426}\text{--}10^{-427}\text{--}10^{-428}\text{--}10^{-429}\text{--}10^{-430}\text{--}10^{-431}\text{--}10^{-432}\text{--}10^{-433}\text{--}10^{-434}\text{--}10^{-435}\text{--}10^{-436}\text{--}10^{-437}\text{--}10^{-438}\text{--}10^{-439}\text{--}10^{-440}\text{--}10^{-441}\text{--}10^{-442}\text{--}10^{-443}\text{--}10^{-444}\text{--}10^{-445}\text{--}10^{-446}\text{--}10^{-447}\text{--}10^{-448}\text{--}10^{-449}\text{--}10^{-450}\text{--}10^{-451}\text{--}10^{-452}\text{--}10^{-453}\text{--}10^{-454}\text{--}10^{-455}\text{--}10^{-456}\text{--}10^{-457}\text{--}10^{-458}\text{--}10^{-459}\text{--}10^{-460}\text{--}10^{-461}\text{--}10^{-462}\text{--}10^{-463}\text{--}10^{-464}\text{--}10^{-465}\text{--}10^{-466}\text{--}10^{-467}\text{--}10^{-468}\text{--}10^{-469}\text{--}10^{-470}\text{--}10^{-471}\text{--}10^{-472}\text{--}10^{-473}\text{--}10^{-474}\text{--}10^{-475}\text{--}10^{-476}\text{--}10^{-477}\text{--}10^{-478}\text{--}10^{-479}\text{--}10^{-480}\text{--}10^{-481}\text{--}10^{-482}\text{--}10^{-483}\text{--}10^{-484}\text{--}10^{-485}\text{--}10^{-486}\text{--}10^{-487}\text{--}10^{-488}\text{--}10^{-489}\text{--}10^{-490}\text{--}10^{-491}\text{--}10^{-492}\text{--}10^{-493}\text{--}10^{-494}\text{--}10^{-495}\text{--}10^{-496}\text{--}10^{-497}\text{--}10^{-498}\text{--}10^{-499}\text{--}10^{-500}\text{--}10^{-501}\text{--}10^{-502}\text{--}10^{-503}\text{--}10^{-504}\text{--}10^{-505}\text{--}10^{-506}\text{--}10^{-507}\text{--}10^{-508}\text{--}10^{-509}\text{--}10^{-510}\text{--}10^{-511}\text{--}10^{-512}\text{--}10^{-513}\text{--}10^{-514}\text{--}10^{-515}\text{--}10^{-516}\text{--}10^{-517}\text{--}10^{-518}\text{--}10^{-519}\text{--}10^{-520}\text{--}10^{-521}\text{--}10^{-522}\text{--}10^{-523}\text{--}10^{-524}\text{--}10^{-525}\text{--}10^{-526}\text{--}10^{-527}\text{--}10^{-528}\text{--}10^{-529}\text{--}10^{-530}\text{--}10^{-531}\text{--}10^{-532}\text{--}10^{-533}\text{--}10^{-534}\text{--}10^{-535}\text{--}10^{-536}\text{--}10^{-537}\text{--}10^{-538}\text{--}10^{-539}\text{--}10^{-540}\text{--}10^{-541}\text{--}10^{-542}\text{--}10^{-543}\text{--}10^{-544}\text{--}10^{-545}\text{--}10^{-546}\text{--}10^{-547}\text{--}10^{-548}\text{--}10^{-549}\text{--}10^{-550}\text{--}10^{-551}\text{--}10^{-552}\text{--}10^{-553}\text{--}10^{-554}\text{--}10^{-555}\text{--}10^{-556}\text{--}10^{-557}\text{--}10^{-558}\text{--}10^{-559}\text{--}10^{-560}\text{--}10^{-561}\text{--}10^{-562}\text{--}10^{-563}\text{--}10^{-564}\text{--}10^{-565}\text{--}10^{-566}\text{--}10^{-567}\text{--}10^{-568}\text{--}10^{-569}\text{--}10^{-570}\text{--}10^{-571}\text{--}10^{-572}\text{--}10^{-573}\text{--}10^{-574}\text{--}10^{-575}\text{--}10^{-576}\text{--}10^{-577}\text{--}10^{-578}\text{--}10^{-579}\text{--}10^{-580}\text{--}10^{-581}\text{--}10^{-582}\text{--}10^{-583}\text{--}10^{-584}\text{--}10^{-585}\text{--}10^{-586}\text{--}10^{-587}\text{--}10^{-588}\text{--}10^{-589}\text{--}10^{-590}\text{--}10^{-591}\text{--}10^{-592}\text{--}10^{-593}\text{--}10^{-594}\text{--}10^{-595}\text{--}10^{-596}\text{--}10^{-597}\text{--}10^{-598}\text{--}10^{-599}\text{--}10^{-600}\text{--}10^{-601}\text{--}10^{-602}\text{--}10^{-603}\text{--}10^{-604}\text{--}10^{-605}\text{--}10^{-606}\text{--}10^{-607}\text{--}10^{-608}\text{--}10^{-609}\text{--}10^{-610}\text{--}10^{-611}\text{--}10^{-612}\text{--}10^{-613}\text{--}10^{-614}\text{--}10^{-615}\text{--}10^{-616}\text{--}10^{-617}\text{--}10^{-618}\text{--}10^{-619}\text{--}10^{-620}\text{--}10^{-621}\text{--}10^{-622}\text{--}10^{-623}\text{--}10^{-624}\text{--}10^{-625}\text{--}10^{-626}\text{--}10^{-627}\text{--}10^{-628}\text{--}10^{-629}\text{--}10^{-630}\text{--}10^{-631}\text{--}10^{-632}\text{--}10^{-633}\text{--}10^{-634}\text{--}10^{-635}\text{--}10^{-636}\text{--}10^{-637}\text{--}10^{-638}\text{--}10^{-639}\text{--}10^{-640}\text{--}10^{-641}\text{--}10^{-642}\text{--}10^{-643}\text{--}10^{-644}\text{--}10^{-645}\text{--}10^{-646}\text{--}10^{-647}\text{--}10^{-648}\text{--}10^{-649}\text{--}10^{-650}\text{--}10^{-651}\text{--}10^{-652}\text{--}10^{-653}\text{--}10^{-654}\text{--}10^{-655}\text{--}10^{-656}\text{--}10^{-657}\text{--}10^{-658}\text{--}10^{-659}\text{--}10^{-660}\text{--}10^{-661}\text{--}10^{-662}\text{--}10^{-663}\text{--}10^{-664}\text{--}10^{-665}\text{--}10^{-666}\text{--}10^{-667}\text{--}10^{-668}\text{--}10^{-669}\text{--}10^{-670}\text{--}10^{-671}\text{--}10^{-672}\text{--}10^{-673}\text{--}10^{-674}\text{--}10^{-675}\text{--}10^{-676}\text{--}10^{-677}\text{--}10^{-678}\text{--}10^{-679}\text{--}10^{-680}\text{--}10^{-681}\text{--}10^{-682}\text{--}10^{-683}\text{--}10^{-684}\text{--}10^{-685}\text{--}10^{-686}\text{--}10^{-687}\text{--}10^{-688}\text{--}10^{-689}\text{--}10^{-690}\text{--}10^{-691}\text{--}10^{-692}\text{--}10^{-693}\text{--}10^{-694}\text{--}10^{-695}\text{--}10^{-696}\text{--}10^{-697}\text{--}10^{-698}\text{--}10^{-699}\text{--}10^{-700}\text{--}10^{-701}\text{--}10^{-702}\text{--}10^{-703}\text{--}10^{-704}\text{--}10^{-705}\text{--}10^{-706}\text{--}10^{-707}\text{--}10^{-708}\text{--}10^{-709}\text{--}10^{-710}\text{--}10^{-711}\text{--}10^{-712}\text{--}10^{-713}\text{--}10^{-714}\text{--}10^{-715}\text{--}10^{-716}\text{--}10^{-717}\text{--}10^{-718}\text{--}10^{-719}\text{--}10^{-720}\text{--}10^{-721}\text{--}10^{-722}\text{--}10^{-723}\text{--}10^{-724}\text{--}10^{-725}\text{--}10^{-726}\text{--}10^{-727}\text{--}10^{-728}\text{--}10^{-729}\text{--}10^{-730}\text{--}10^{-731}\text{--}10^{-732}\text{--}10^{-733}\text{--}10^{-734}\text{--}10^{-735}\text{--}10^{-736}\text{--}10^{-737}\text{--}10^{-738}\text{--}10^{-739}\text{--}10^{-740}\text{--}10^{-741}\text{--}10^{-742}\text{--}10^{-$

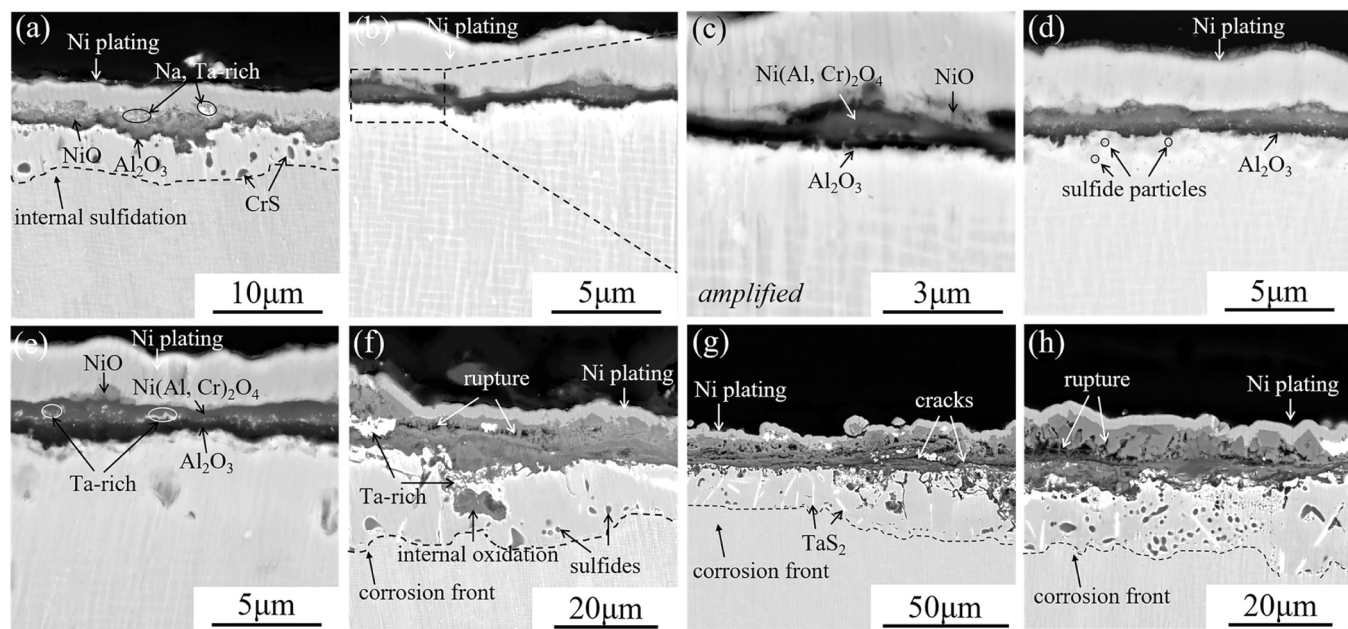


**Fig. 12.** Cross-sectional morphologies of the specimens after hot corrosion at 850 °C in 75 wt% Na<sub>2</sub>SO<sub>4</sub> + 25 wt% K<sub>2</sub>SO<sub>4</sub> molten salts for 30 h: (a) 0<sup>sub</sup>, (b) 1<sup>20 h</sup>, (c) the amplified view of (b), (d) 2<sup>20 h</sup>, (e) 2<sup>100 h</sup>, (f) 2<sup>100 h</sup>, (g) 3<sup>20 h</sup>, (h) 3<sup>100 h</sup>.



The failure of the protective Al<sub>2</sub>O<sub>3</sub> scale was thus accelerated as shown in Fig. 10. Combined with the distribution of O and the XRD patterns in Fig. 6, these Ta-rich compounds were proven to be NaTaO<sub>3</sub>. The scale was porous and contained multiple oxides rich in Ta, Al, Ni and Cr.

When the surface scale became loose and porous, the molten salts penetrated through the nonprotective scale into the substrate, and inner sulfidation occurred. Due to the lower critical oxygen partial pressure and the lower standard free energy to form Ta-rich sulfides than that of CrS and Ni<sub>3</sub>S<sub>2</sub> [31], TaS<sub>2</sub> could easily form in the inner sulfide layer. In the present experiment, Ni<sub>3</sub>S<sub>2</sub> and Ni-Ni<sub>3</sub>S<sub>2</sub> eutectics with low melting points tended to form beneath the corrosion scale [10,45]. CrS and TaS<sub>2</sub> formed a deeper internal sulfide layer, indicating the depth of the corrosion front. CrS and TaS<sub>2</sub> always coexisted, but the amount and distribution varied from 30 h to 60 h of corrosion (Fig. 8 and Fig. 12). It could be observed from element mapping by EPMA in Fig. 10 that Cr/Ta compounds dominated beneath the outer NiO scale with discontinuously distributed Al<sub>2</sub>O<sub>3</sub>. The existence of mixed Ta/Cr-rich compounds

was not only nonprotective but also served as a “block” occupying the location for Al<sub>2</sub>O<sub>3</sub> to grow. Therefore, internal oxidation of Al occurred, and the Al<sub>2</sub>O<sub>3</sub> was severely disrupted by the Ta/Cr-rich compounds, reducing its protection.

Taking the 3<sup>100 h</sup> specimen group as an example, the corrosion degradation process is given by a schematic diagram in Fig. 13. As shown in the figure, after preoxidation, multiple oxide scales with the outer NiO and Ni-Al/Cr spinel and inner Al<sub>2</sub>O<sub>3</sub> form on the surface of the alloy. At the same time, some Ta oxides form within the scale, which causes some scale defects (Fig. 13(a)). After corrosion, the scales are dissolved by molten salt. The Ta oxides are also dissolved in the molten salt by generating a compound of NaTaO<sub>3</sub>. As a result, the scale becomes loose with obvious holes. As the corrosion process proceeds, NaTaO<sub>3</sub> segregates in the scale and is dominant in the inner zone beneath the outer loose NiO, while the Al-depleted zone becomes larger in the substrate. Therefore, continuous protective Al<sub>2</sub>O<sub>3</sub> is unable to form, and only inner discontinuous Al<sub>2</sub>O<sub>3</sub> split by Ta/Cr compounds forms. Because the scale loses protectiveness, the interior sulfidation became significant, and the interior sulfides of Cr and Ta are developed beneath the scale. The corrosion front is moving to a deeper interior of the

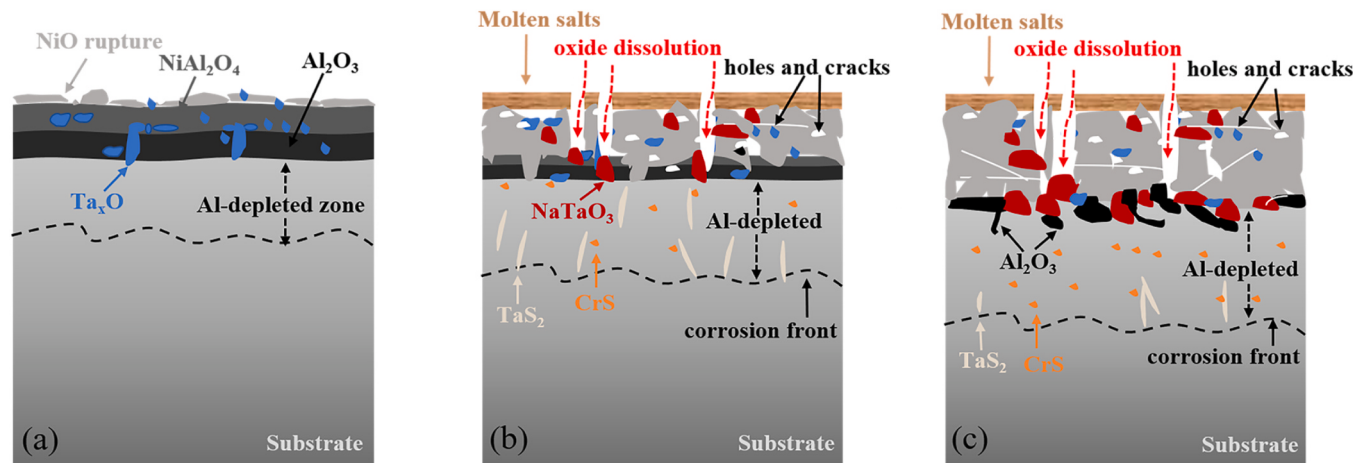


**Fig. 13.** Simple schematic diagrams of the corrosion degradation mechanism for 3<sup>100 h</sup>: (a) after preoxidation; (b) and (c) corrosion process.

substrate where CrS and TaS<sub>2</sub> form.

## 5. Conclusions

The hot corrosion behavior of the SC superalloy N5 with different preoxidation treatments coated with Na<sub>2</sub>SO<sub>4</sub> + 25 wt% K<sub>2</sub>SO<sub>4</sub> was studied at 850 °C. Based on the above study, the following conclusions can be drawn:

During corrosion, the original N5 alloy (0<sup>sub</sup>) showed a certain corrosion resistance for a short reaction time but failed after increasing reaction time. After corrosion for 60 h, its oxide scale mainly consisted of an outer porous NiO and an inner thin and discontinuous Al<sub>2</sub>O<sub>3</sub>, accounting mainly for the low corrosion resistance.

The 2<sup>100</sup> h, 3<sup>20</sup> h and 3<sup>100</sup> h performed severe corrosion even for a short reaction time. For these samples, the oxide scales mainly consisted of NiO and Ni-Al/Cr spinels with massive pores and cracks. As the basic fluxing of oxide scale into the molten sulfate, continuous Al<sub>2</sub>O<sub>3</sub> could not form due to excessive pre-consumed content of Al during preoxidation. Massive Ta oxide segregation ruined the compactness of the preformed oxide scale, and the fast dissolution of such Ta oxides into molten salts accelerated the degradation of the oxide scales.

The 2<sup>20</sup> h performed better than the original N5 alloy after corrosion. Its oxide scale consisted of relatively dense NiO and Ni-Al/Cr spinels. Less pre-consumed Al and Ta-oxide segregation contributed to better corrosion resistance.

The 1<sup>20</sup> h and 1<sup>100</sup> h exhibited the best corrosion resistance. The oxide scale consisted of an outer NiO, a middle NiAl<sub>2</sub>O<sub>4</sub> and an inner continuous Al<sub>2</sub>O<sub>3</sub>, which remain no significant change after corrosion. Sufficient Al supply ensured the formation of a continuous inner protective Al<sub>2</sub>O<sub>3</sub> layer. There was no obvious adverse effect of Ta, accounting for the improved corrosion resistance.

## CRediT authorship contribution statement

**Xiaowen Yang:** Methodology, Conceptualization, Formal analysis, Visualization, Writing – original draft. **Lanlan Yang, Zehao Chen:** Methodology, Writing – original draft. **Jinlong Wang, Minghui Chen:** Funding acquisition, Supervision, Project administration, Writing – review & editing. **Jianqiang Zhang:** Supervision, Writing – review & editing. **Fuhui Wang:** Supervision.

## Declaration of Competing Interest

The authors declare that they have no known competing financial interests or personal relationships that could have appeared to influence the work reported in this paper.

## Data availability

All data included in this study are available upon request by contact with the corresponding author.

## Acknowledgements

This project is financially supported by the National Natural Science Foundation of China under Grant (Nos. 51671053 and 51801021), the National Key R&D Program of China under Grant (No. 2017YFB0306100), the Fundamental Research Funds for the Central Universities (No. N2102015 and N2302007), and by the Ministry of Industry and Information Technology Project (No. MJ-2017-J-99).

## References

- [1] R.A. Rapp, Hot corrosion of materials: a fluxing mechanism? *Corros. Sci.* 44 (2002) 209–221.
- [2] N.E. Paton, W.M. Robertson, F. Mansfeld, High temperature behavior of superalloys exposed to sodium chloride: I. mechanical properties, *Mater. Trans. B* 4 (1973) 317–320.
- [3] D.M. Johnson, D.P. Whittle, J. Stringer, Mechanisms of Na<sub>2</sub>SO<sub>4</sub>-induced accelerated oxidation, *Corros. Sci.* 15 (1975) 721–739.
- [4] P. Knutsson, H. Lai, K. Stiller, A method for investigation of hot corrosion by gaseous Na<sub>2</sub>SO<sub>4</sub>, *Corros. Sci.* 73 (2013) 230–236.
- [5] N. Eliaz, G. Shemesh, R.M. Latanision, Hot corrosion in gas turbine components, *Eng. Fail. Anal.* 9 (2002) 31–43.
- [6] D.M. Lloyd, High temperature corrosion of superalloys, *High Temp. Technol.* 4 (1986) 107–111.
- [7] X. Montero, A. Ishida, T.M. Meinhard, H. Murakami, M.C. Galetz, Effect of surface treatment and crystal orientation on hot corrosion of a Ni-based single-crystal superalloy, *Corros. Sci.* 166 (2020).
- [8] P. Song, M.F. Liu, X.W. Jiang, Y.C. Feng, J.J. Wu, G. Zhang, D. Wang, J.S. Dong, X.Q. Chen, L.H. Lou, Influence of alloying elements on hot corrosion resistance of nickel-based single crystal superalloys coated with Na<sub>2</sub>SO<sub>4</sub> salt at 900°C, *Mater. Des.* 197 (2021).
- [9] G. Prashar, H. Vasudev, Hot corrosion behavior of superalloys, *Mater. Today Proc.* 26 (2020) 1131–1135.
- [10] Q.X. Fan, S.M. Jiang, H.J. Yu, J. Gong, C. Sun, Microstructure and hot corrosion behaviors of two Co modified aluminide coatings on a Ni-based superalloy at 700°C, *Appl. Surf. Sci.* 311 (2014) 214–223.
- [11] P. Lortakul, R.W. Trice, K.P. Trumble, M.A. Dayananda, Investigation of the mechanisms of Type-II hot corrosion of superalloy CMSX-4, *Corros. Sci.* 80 (2014) 408–415.
- [12] W.Y. Sun, J.L. Wang, L.L. Yang, M.H. Chen, Z.B. Bao, C.Y. Zheng, S.L. Zhu, F.H. Wang, Studies on corrosion behavior of a single-crystal superalloy and its sputtered nanocrystalline coatings with solid NaCl deposit in O<sub>2</sub> + 38 vol% H<sub>2</sub>O environment at 700°C, *Corros. Sci.* 161 (2019).
- [13] Z.H. Chen, T. Dong, W.W. Qu, Y. Ru, H. Zhang, Y.L. Pei, S.K. Gong, S.S. Li, Influence of Cr content on hot corrosion and a special tube sealing test of single crystal nickel base superalloy, *Corros. Sci.* 156 (2019) 161–170.
- [14] M.H. Li, X.F. Sun, W.Y. Hu, H.R. Guan, S.G. Chen, Hot corrosion of a single crystal Ni-base superalloy by Na-salts at 900°C, *Oxid. Met.* 65 (2006) 137–150.
- [15] Z.B. Bao, Q.M. Wang, W.Z. Li, X. Liu, J. Gong, T.Y. Xiong, C. Sun, Preparation and hot corrosion behaviour of an Al-gradient NiCoCrAlYSiB coating on a Ni-base superalloy, *Corros. Sci.* 51 (2009) 860–867.
- [16] L.J. Zhu, S.L. Zhu, F.H. Wang, Hot corrosion behaviour of a Ni+CrAlYSiN composite coating in Na<sub>2</sub>SO<sub>4</sub>-25 wt% NaCl melt, *Appl. Surf. Sci.* 268 (2013) 103–110.
- [17] H.Y. Wang, D.W. Zuo, G. Chen, G.F. Sun, X.F. Li, X. Cheng, Hot corrosion behaviour of low Al NiCoCrAlY cladded coatings reinforced by nano-particles on a Ni-base superalloy, *Corros. Sci.* 52 (2010) 3561–3567.
- [18] X. Ren, F. Wang, High-temperature oxidation and hot-corrosion behavior of a sputtered NiCrAlY coating with and without aluminizing, *Surf. Coat. Technol.* 201 (2006) 30–37.
- [19] T.S. Sidhu, S. Prakash, R.D. Agrawal, Evaluation of hot corrosion resistance of HVOF coatings on a Ni-based superalloy in molten salt environment, *Mater. Sci. Eng. A* 430 (2006) 64–78.
- [20] L.C. Chen, C. Zhang, Z.G. Yang, Effect of pre-oxidation on the hot corrosion of CoNiCrAlYRe alloy, *Corros. Sci.* 53 (2011) 374–380.
- [21] G.M. Liu, F. Yu, J.H. Tian, J.H. Ma, Influence of pre-oxidation on the hot corrosion of M38G superalloy in the mixture of Na<sub>2</sub>SO<sub>4</sub>-NaCl melts, *Mater. Sci. Eng. A* 496 (2008) 40–44.
- [22] E.Z. Liu, Z. Zheng, X.R. Guan, J. Tong, L.K. Ning, Y.S. Yu, Influence of pre-oxidation on the hot corrosion of DZ68 superalloy in the mixture of Na<sub>2</sub>SO<sub>4</sub>-NaCl, *J. Mater. Sci. Technol.* 26 (2010) 895–899.
- [23] H.T. Mallikarjuna, N.L. Richards, W.F. Caley, Isothermal oxidation comparison of three Ni-based superalloys, *J. Mater. Eng. Perform.* 26 (2017) 2014–2023.
- [24] M. Brossard, B. Bouchaud, G. Bonnet, B. Rannou, F. Pedraza, Early stages of high temperature cyclic oxidation of an electrodeposited ceria coating on nickel superalloys under water-drop tests, *Oxid. Met.* 81 (2013) 95–104.
- [25] M. Bensch, A. Sato, N. Warnken, E. Affeldt, R.C. Reed, U. Glatzel, Modelling of high temperature oxidation of alumina-forming single-crystal nickel-base superalloys, *Acta Mater.* 60 (2012) 5468–5480.
- [26] M. Bensch, J. Preußner, R. Hüttner, G. Obigodi, S. Virtanen, J. Gabel, U. Glatzel, Modelling and analysis of the oxidation influence on creep behaviour of thin-walled structures of the single-crystal nickel-base superalloy René N5 at 980°C, *Acta Mater.* 58 (2010) 1607–1617.
- [27] J.L. Wang, M.H. Chen, S.L. Zhu, F.H. Wang, Ta effect on oxidation of a nickel-based single-crystal superalloy and its sputtered nanocrystalline coating at 900–1100°C, *Appl. Surf. Sci.* 345 (2015) 194–203.
- [28] L.L. Yang, J.L. Wang, R.Z. Yang, S.S. Yang, Y.X. Jia, M.H. Chen, Y.X. Qiao, P.Y. Guo, S.L. Zhu, F.H. Wang, Oxidation behavior of a nanocrystalline coating with low Ta content at high temperature, *Corros. Sci.* 180 (2021).
- [29] L.L. Yang, M.H. Chen, J.L. Wang, Z.B. Bao, S.L. Zhu, F.H. Wang, Diffusion of Ta and its influence on oxidation behavior of nanocrystalline coatings with different Ta, Y and Al contents, *Corros. Sci.* 126 (2017) 344–355.
- [30] G.C. Fryburg, C.A. Stearns, F.J. Koijl, Mechanism of beneficial effect of tantalum in hot corrosion of nickel-base superalloys, *J. Electrochem Soc.* 124 (1977) 1147–1149.

- [31] J.X. Chang, D. Wang, T. Liu, G. Zhang, L.H. Lou, J. Zhang, Role of tantalum in the hot corrosion of a Ni-base single crystal superalloy, *Corros. Sci.* 98 (2015) 585–591.
- [32] J.X. Chang, D. Wang, G. Zhang, L.H. Lou, J. Zhang, Interaction of Ta and Cr on type-I hot corrosion resistance of single crystal Ni-base superalloys, *Corros. Sci.* 117 (2017) 35–42.
- [33] J.L. Wang, M.H. Chen, Y.X. Cheng, L.L. Yang, Z.B. Bao, L. Liu, S.L. Zhu, F.H. Wang, Hot corrosion of arc ion plating NiCrAlY and sputtered nanocrystalline coatings on a nickel-based single-crystal superalloy, *Corros. Sci.* 123 (2017) 27–39.
- [34] J.S. Zhang, Z.Q. Hu, Y. Murata, M. Morinaga, N. Yukawa, Design and development of hot corrosion-resistant nickel-base single-crystal superalloys by the d-electrons alloy design theory. 2. Effects of refractory-metals Ti, Ta, and Nb on microstructures and properties, *Metall. Trans. A* 24 (1993) 2451–2464.
- [35] H. Cui, J.S. Zhang, Y. Murata, M. Morinaga, N. Yukawa, Hot corrosion behavior of Ni-based superalloy with high Cr contents-part 1. Experimental study, *J. Univ. Sci. Technol. Beijing (Engl. Ed.)* 2 (1996) 84–89.
- [36] T. Perez, D. Monceau, C. Desgranges, Kinetic oxidation model including the transient regime for a single crystal nickel-based superalloy over the temperature range 750–1300°C, *Corros. Sci.* 206 (2022).
- [37] Edward L. Simons, George V. Browning, H.A. Liebhafsky, Sodium sulfate in gas turbines, *Corrosion* 11 (1955) 17–26.
- [38] C. Leyens, B.A. Pint, I.G. Wright, Effect of composition on the oxidation and hot corrosion resistance of NiAl doped with precious metals, *Surf. Coat. Technol.* 133–134 (2000) 15–22.
- [39] J. Stringer, High-temperature corrosion of superalloys, *Mater. Sci. Technol.* 3 (1987) 482–493.
- [40] M.H. Li, Z.Y. Zhang, X.F. Sun, J.G. Li, F.S. Yin, W.Y. Hu, H.R. Guan, Z.Q. Hu, Oxidation behavior of sputter-deposited NiCrAlY coating, *Surf. Coat. Technol.* 165 (2003) 241–247.
- [41] C. Wagner, Theoretical analysis of the diffusion process determining the oxidation rate of alloys, *J. Electrochem. Soc.* 99 (1952) 369–380.
- [42] C. Wagner, Reaktionstypen bei der oxydation von legierungen, *Z. Für Elektrochem.* 63 (1959) 772–790.
- [43] H. Singh, D. Puri, S. Prakash, T.K. Ghosh, Hot corrosion of a plasma sprayed Ni<sub>3</sub>Al coating on a Ni-base superalloy, *Mater. Corros.* 58 (2007) 857–866.
- [44] S.J. Geng, F.H. Wang, S.L. Zhu, W. Wu, Hot-corrosion resistance of a sputtered K38G nanocrystalline coating in molten sulfate at 900°C, *Oxid. Met* 57 (2002) 549–557.
- [45] G. Goward, Protective coatings - purpose, role, and design, *Mater. Sci. Technol.* 2 (1986) 194–200.